https://doi.org/10.5194/egusphere-2026-6752
Preprint. Discussion started: 6 November 2026
© Author(s) 2026. CC BY 4.0 License.

Temperature modulates sediment priming triggered by simulated algal blooms: Insights from sediment microbial fuel cells

Wenfeng Ning[a], Jinjun Kan[b], Guangchao Zhuang[c], Prakhin Assavapanuvat[d], Patricia Bonin[e], Thomas Bianchi[f,g], Jean-François Rontani[e], Guipeng Yang[c], Hui Zhang[h], Xinxin Li[a,*]

[a] Department of Ocean Science and Engineering, Southern University of Science and Technology, Shenzhen 518055, China

[b] Stroud Water Research Center, Avondale, Pennsylvania 19311, USA

[c] College of Chemistry and Chemical Engineering, Ocean University of China, Qingdao 266100, China

[d] Department of Geology, Chulalongkorn University, Bangkok 10330, Thailand

[e] Aix Marseille Univ, Université de Toulon, CNRS, IRD, MIO UM 110, 13288 Marseille, France

[f] Institute for the Study of Earth, Oceans, and Space (EOS), University of New Hampshire, Durham, New Hampshire 03824, USA

[g] Department of Geological Sciences, University of Florida, Gainesville, Florida 32611-2120, USA

[h] Shenzhen Natural Resources and Real Estate Evaluation and Development Research Center, Shenzhen 518034, China

[*] Corresponding author

E-mail address: lixinxin@sustech.edu.cn

https://doi.org/10.5194/egusphere-2026-6752
Preprint. Discussion started: 6 November 2026
© Author(s) 2026. CC BY 4.0 License.

Highlights

1. SMFC provides a real-time tool for tracking sediment redox processes and microbial electrogenic activity.
2. Warming decouples intrinsic SOC mineralization from priming-driven turnover in mangrove sediments.
3. Priming shifts from weakly negative to strongly positive across 25–35 °C.
4. Anoxic extracellular electron transfer sustained by an active anode drives late-stage lignin phenol degradation.

https://doi.org/10.5194/egusphere-2026-6752
Preprint. Discussion started: 6 November 2026
© Author(s) 2026. CC BY 4.0 License.

Abstract

Mangrove sediments are major blue carbon reservoirs, yet how warming and eutrophication interact to control the stability of sediment organic carbon (SOC) remains uncertain. Here, we combined sediment microbial fuel cell (SMFC) monitoring with (in)organic carbon analyses, and lignin biomarker measurements in ^{13}C-labeled algal-amended subtropical mangrove sediments to investigate temperature-dependent priming of SOC at 25, 30, and 35 ℃. Baseline SOC mineralization exhibited a nonlinear increase across the 25–30 °C thermal range, followed by a distinct decline at 35 °C. In contrast, priming intensity increased progressively with increasing temperature, shifting from weakly negative to strongly positive. This divergence reveals that warming decouples intrinsic SOC mineralization from priming-driven carbon turnover. Mechanistically, algal inputs provided energetic sources that activated opportunistic copiotrophs (*Bacteroidota*) and restructured anodic interactomes by enriching syntrophic microorganisms (e.g., *Anaerolineaceae*, *Desulfosarcinaceae*). Rather than relying on obligate aerobes, late-stage oxidative cleavage of recalcitrant lignin phenols was sustained under anoxic conditions by the active anode, which served as an inexhaustible electron sink via extracellular electron transfer. These findings suggest that warming shifts microbial metabolisms rather than uniformly stimulating carbon mineralization, promoting the priming degradation of otherwise stable SOC. Consequently, warming may disproportionately increase the vulnerability of stabilized SOC in eutrophic mangrove ecosystems by amplifying priming effects relative to baseline mineralization. Incorporating temperature-dependent priming into blue carbon models may improve predictions of coastal carbon storage under future climate change.

Keywords: Mangrove sediments, Sediment microbial fuel cell, Warming, Algal bloom, Organic carbon, Priming effect.

https://doi.org/10.5194/egusphere-2026-6752
Preprint. Discussion started: 6 November 2026
© Author(s) 2026. CC BY 4.0 License.

1. Introduction

Coastal mangroves are among the most efficient natural carbon sinks, storing disproportionately large amounts of sediment organic carbon (SOC) relative to their global area (Alongi, 2014; Donato et al., 2011). The long-term preservation of this blue carbon (e.g., salt marshes, mangroves, and seagrasses) reservoir plays a crucial role in regulating atmospheric CO_2 concentrations and buffering climate warming (Ali et al., 2025; Macreadie et al., 2019). Mangrove sediments receive continuous inputs of terrestrial and marine organic matter, creating highly heterogeneous biogeochemical environments that influence SOC transformation and persistence. These carbon stocks are vulnerable to environmental perturbations (Guo et al., 2024; Regnier et al., 2022), with microbial processes playing a central role in determining whether SOC is preserved or mineralized (Bonin et al., 2023).

The frequency and magnitude of algal blooms in many subtropical estuaries have increased as a result of anthropogenic nutrient enrichment (Malone and Newton, 2020; Paerl et al., 2014). These episodic pulses of labile organic carbon may accelerate the decomposition of native, lignin-rich refractory SOC derived from mangrove vegetation (Nie et al., 2026) through the "priming effect" (Guenet et al., 2010; Bianchi, 2011). This phenomenon, characterized by an accelerated mineralization (typically by 10% to 30%) of stable, low-reactivity organic matter stimulated by the concurrent decomposition of highly labile inputs, has been documented across terrestrial soils, aquatic sediments, and natural waters (Löhnis, 1926; van Nugteren et al., 2009; Danger et al., 2013; Bianchi et al., 2015). For instance, recent work has shown that adding algal lipids accelerated indigenous SOC degradation by 2.5 to 6 times (Zhu et al., 2024). However, studies have also reported negative priming effects (Gontikaki et al., 2013; Bengtsson et al., 2018), or negligible responses (Bengtsson et al., 2014; Catalán et al., 2015), suggesting that the direction and magnitude of priming may depend strongly on environmental context (see Bengtsson et al., 2018). Unfortunately, the potential of priming effects has been largely overlooked in coastal carbon burial "hotspots" (Bianchi et al., 2018). In particular, the priming effect in coastal habitats such as mangrove sediments, characterized by fluctuating oxygen availability (e.g., Aller and Cochran, 2019) and high inputs of structurally complex terrestrial organic carbon, remains poorly understood. Furthermore, while recent studies have shown that global warming may reduce priming effects in soils (Dong et al., 2024; Li et al., 2023), the impact of temperature on priming in sedimentary systems remains elusive.

Warming may alter the sediment carbon balance by either favoring degradation of fresh algal inputs (suppressing native organic carbon loss) or by stimulating the breakdown of old, refractory carbon. Because baseline mineralization and priming responses exhibit different thermal sensitivities, warming could decouple intrinsic respiration from priming-driven carbon destabilization (Dong et al., 2024; Li et al., 2023). Resolving these temperature-dependent dynamics is crucial for assessing mangrove carbon vulnerability under concurrent warming and eutrophication. However, traditional discrete greenhouse gas measurements often miss or fail to capture these rapid and transient shifts in substrate utilization (e.g., Gontikaki et al., 2015; Yang et al., 2022). Sediment microbial fuel cells (SMFCs) provide a continuous, high-

https://doi.org/10.5194/egusphere-2026-6752
Preprint. Discussion started: 6 November 2026
© Author(s) 2026. CC BY 4.0 License.

resolution bio-electrochemical platform for monitoring real-time current output, integrating the metabolic activities of diverse electroactive microbial communities and their distinct electron-transfer pathways during SOC turnover (Kan et al. 2011; Reimers et al. 2001; Tender et al. 2002; Hong et al. 2010). Combined with stable isotope tracing and geochemical biomarkers, this approach enables mechanistic tracking of carbon flow, substrate partitioning, and priming-induced changes in SOC mineralization throughout incubation.

In this study, we investigated temperature-dependent SOC mineralization and algal-induced priming effects in subtropical mangrove sediments using controlled incubations at 25, 30, and 35 °C. By introducing ^{13}C-labeled algal organic matter into SMFCs systems, we combined continuous bio-electrochemical monitoring with the isotopic partitioning of dissolved inorganic carbon (DIC), lignin-derived phenols (Λ_8), and microbial community analysis to distinguish baseline SOC mineralization from priming-induced decomposition of native SOC. Specifically, we addressed two central scientific questions: (i) How does warming regulate baseline mineralization in mangrove sediments? and (ii) How does temperature modulate the occurrence, direction, and magnitude of algal-induced priming effects on native SOC? By resolving the thermal sensitivity and directionality of priming effects in mangrove sediments, this study provides mechanistic insights into how warming and eutrophication interact to regulate the stability of mangrove carbon.

2. Materials and methods

2.1 Study area and sample collection

The Futian Mangrove Nature Reserve (113°56′E-114°3′E, 22°30′N-22°32′N), located at the northeast coast of Shenzhen Bay, Guangdong Province, China, is characterized by a subtropical monsoon climate with a mean annual temperature of 22.4 °C (July: 28.7 °C; January: 14.1 °C) and annual precipitation of 1700-1900 mm. Mangrove vegetation is dominated by native species, including *Kandelia obovata* and *Aegiceras corniculatum*, as well as introduced species such as *Sonneratia apetala* (Li et al., 2025b). Tides are irregular semidiurnal, exhibiting marked tidal inequality and a relatively small tidal range of 1.4 m (Feng et al., 2020). The combined influences of riverine inputs and tidal forcing promote the accumulation of fine-grained sediments and nutrient loading within the preserve, resulting in persistent eutrophication conditions (Yan et al., 2021). Notably, 189 harmful algal bloom events have been reported off Shenzhen coasts between 1980 and 2018, of which 25.4% occurred in the Pearl River Estuary and the northwestern part of Shenzhen Bay (Xu et al., 2018).

Surface sediments (0–5 cm depth) were collected at low tides from a *Kandelia obovata* wetland (22°31′N, 114°00′E; Fig. S1) in October 2023. Roots and debris were removed from the sediment. The samples were then transported to the laboratory in a portable cooler at 4 °C. To minimize potential bias from sample heterogeneity, all sediments were thoroughly homogenized in the laboratory prior to incubation experiments.

https://doi.org/10.5194/egusphere-2026-6752
Preprint. Discussion started: 6 November 2026
© Author(s) 2026. CC BY 4.0 License.



2.2 Sediment microbial fuel cells (SMFCs) construction, incubation, and sampling

Carbon cloths were used as the cathode (5 × 5 cm) and anode (7 × 7 cm) materials for SMFCs. The anode array was connected to the cathode with rubber-sealed copper wire (Φ 0.6 mm), and all bonding sites were covered with silicone rubber to prevent corrosion. Three sets of SMFCs were established in 500 mL glass bottles sealed with butyl rubber stoppers for incubation under three temperature regimes (Fig. 1): low (L, 25 ± 0.5 ℃, representing typical warm-season sediment conditions(Zhu et al., 2023)), mid (M, 30 ± 0.5℃, reflecting end-of-century warming under the RCP 8.5 scenario(IPCC, 2022)), and high (H, 35 ± 0.5℃, simulating extreme thermal anomalies compounded by global warming (Sang et al., 2026)). Each bottle contained 250 mL of wet mangrove sediment and 250 mL of 35‰-sterilized artificial seawater, with cathodes positioned in the overlying water and anodes embedded in the sediment. All systems were pre-incubated in dark, temperature-controlled chambers under open-circuit conditions to allow microbial stabilization and thermal acclimation. The pre-incubation was conducted for 6 days at 25 and 5 days at 30 °C, and for 4 days at 35 °C.

Once the open-circuit potential between the electrodes stabilized (measured with a high-performance digital multimeter, model VICTOR VC890D), indicating successful microbial attachment and stable electroactive biofilm formation on the anode, SMFCs were connected to a 1,000 Ω external resistor. To simulate pulse inputs of labile organic matter during eutrophication events, 0.2 g of ^{13}C-labeled lyophilized algal cells (^{13}C abundance: 83.29 atom %; $\delta^{13}C_{VPDB}$ = 444,739.29‰; product no. CLM-2085-1; Cambridge Isotope Laboratories, Inc., Andover, MA, USA), suspended in sterilized seawater, was injected into sediments using a syringe. Six treatment combinations were established across 3 incubation temperatures (Fig. 1): (1) Low-temperature control (25 °C; LC); (2) Low-temperature treatment (25 °C + ^{13}C-algae; LT); (3) Mid-temperature control (30 °C; MC); (4) Mid-temperature treatment (30 °C + ^{13}C-algae; MT); (5) High-temperature control (35 °C; HC); (6) High-temperature treatment (35 °C + ^{13}C-algae; HT). To facilitate the cathodic reaction, oxygen was injected into the overlying water twice in all units.

Voltage (U) was recorded by the high-performance digital multimeter, and the current I was then calculated using Ohm's law as $I=U/R$, where U is the potential difference between the cathode and anode, and R is the external resistance (1,000 Ω). Current density (J) under closed-circuit conditions was then normalized to the anode surface area (A=L×D, where L and D represent the anode length and width, respectively):

$$J = I/A \quad (1)$$

Based on the current production, destructive sampling was conducted at multiple time points during the incubation, as shown in Figs. 1 and 2. The sampling days (from the start of the experiment) were days 17 and 31 at 25 °C, days 13, 17, and 36 at 30 °C, and days 10, 12, 18, and 38 at 35°C. The corresponding baseline samples (LC0, MC0, and HC0) were collected after circuit closure but before algal addition. At each sampling time, one bottle from each of the two groups at the corresponding temperature was destructively sampled. Specifically, one control bottle and one algae-amended

https://doi.org/10.5194/egusphere-2026-6752
Preprint. Discussion started: 6 November 2026
© Author(s) 2026. CC BY 4.0 License.

bottle were sampled at each time point at 25 °C (LC and LT), 30 °C (MC and MT), and 35 °C (HC and HT).

Overlying water was filtered through pre-combusted GF/F filters (0.7 μm, Whatman) and stored at -20 °C for particulate organic carbon (POC) analyses. Filtrates were split for dissolved organic carbon (DOC, -20 °C) and dissolved inorganic carbon (DIC)/δ^{13}C-DIC analyses (stored at 4 °C in N_2-flushed vials). Homogenized sediments were divided into subsamples and stored at -80 °C prior to physicochemical and microbial molecular analyses.

2.3 Physicochemical property measurements

***2.3.1 Overlying water*:** POC filters were acid-fumigated (12 N HCl, 12 h) to remove inorganic carbon and subsequently dried at 60 °C for 12 h. Treated filters were encapsulated in tin capsules for the determination of POC contents using a Thermo Scientific Flash 2000 CHN elemental analyzer. Stable carbon isotope ratios δ^{13}C were subsequently measured by coupling the elemental analyzer to an isotope ratio mass spectrometer (IRMS; UC Davis Stable Isotope Facility), with values reported relative to Vienna Pee Dee Belemnite (VPDB; analytical precisions of ±0.2‰).

DOC concentrations were measured by high-temperature catalytic oxidation with a Shimadzu TOC-L analyzer, calibrated with a seven-point standard curve (0-40 mg L^{-1}) and with a coefficient of variation <2% (Halewood et al., 2022). DIC and δ^{13}C-DIC were determined using a Picarro Cavity Ring Down Spectrometer G2201-i isotope analyzer following acidification with 85% phosphoric acid to convert DIC to CO_2 at Ocean University of China.

2.3.2 Sediment: The total organic carbon (TOC, %), total nitrogen (TN, %), δ^{13}C (‰) were analyzed using the same procedure for the POC filters mentioned above.

Dehydrogenase activity (DHA) was determined using the triphenyl tetrazolium chloride (TTC) reduction method (Song and Jiang, 2018). Sediments (7 g) were incubated with TTC (4 g L^{-1}) and Tris-HCl buffer (0.2 mol L^{-1}, pH 8.2) at 37 °C for 12 h. The triphenyl formazan (TPF) produced was extracted with toluene and quantified spectrophotometrically at 485 nm. Results are expressed as TPF production per unit mass and time.

Lignin phenols were extracted via alkaline CuO oxidation (Hedges and Ertel, 1982), derivatized with N,O-Bis-(trimethylsilyl)-trifluoroacetamide (BSTFA), and analyzed by an Agilent 7890 Gas Chromatograph/5977 Mass Spectrometric Detector. Lignin-derived indices included Λ_8 (normalized to OC content, mg 100 mg^{-1} OC) as total lignin phenols normalized to organic carbon, $(Ad/Al)_V$, and $(Ad/Al)_S$ as proxies for oxidative degradation.

2.4 End-member mixing model

The DIC in the overlying water was assumed to originate from three sources: (i) baseline mineralization of native SOC, (ii) mineralization of added ^{13}C-labeled algal organic matter, and (iii) additional (primed) decomposition of SOC stimulated by algal inputs. Therefore, the partitioning of DIC sources within the SMFCs was quantified using a stable carbon isotope end-member mixing model:

$$\Delta C_{total}=C_f - C_i=\Delta C_{Ctrl}+\Delta C_A+\Delta C_{Primed} \quad (2)$$

https://doi.org/10.5194/egusphere-2026-6752
Preprint. Discussion started: 6 November 2026
© Author(s) 2026. CC BY 4.0 License.

where C_i and C_f were the initial and final DIC concentrations, respectively. The C_i value corresponds to the DIC value measured for each treatment after closing the circuit (Fig. 1 and 2). ΔC_{Ctrl} represents DIC production from control sediments under a given temperature, ΔC_A denotes DIC derived from added algal organic matter mineralization, and ΔC_{Primed} represents additional DIC production from sediment induced by priming effects.

The carbon isotopic mass balance of DIC was established as follows:

$$\Delta C_{total} \times \delta^{13}C_{total} = C_f \times \delta^{13}C_f - C_i \times \delta^{13}C_i = \Delta C_{Ctrl} \times \delta^{13}C_{Ctrl} + \Delta C_A \times \delta^{13}C_A + \Delta C_{Primed} \times \delta^{13}C_{Primed} \quad (3)$$

where $\delta^{13}C_i$ and $\delta^{13}C_f$ were the initial and final isotopic compositions of DIC. $\delta^{13}C_{Ctrl}$ and $\delta^{13}C_{Primed}$ represented the isotopic signatures of DIC derived from control and primed SOC, respectively, and $\delta^{13}C_A$ was the isotopic signature of the added algae organic matter $\delta^{13}C_A$ = +444,739.29‰. Assuming that the primed native SOC shares the same carbon isotopic signature as the control sediment, $\delta^{13}C_{Primed} = \delta^{13}C_{Ctrl}$, Eqs. (2) and (3) were solved simultaneously to quantitatively resolve ΔC_A and ΔC_{Primed}.

The mineralization rate of SOC in the control group $M_{Control}$, in μmol C L^{-1} d^{-1}, the mineralization rate of primed SOC (M_{Primed}), and the mineralization rate of algae (M_A) were calculated over the incubation duration (t, in days) as:

$$M_{Control} = \Delta C_{Ctrl} * 1000/t, \quad M_A = \Delta C_A * 1000/t, \quad M_{Primed} = \Delta C_{Primed} * 1000/t \quad (4)$$

To quantify the intensity and direction of priming effects, a priming enhancement factor (PEF) was defined as:

$$PEF = (\Delta C_{Ctrl} + \Delta C_{Primed})/\Delta C_{Ctrl} = 1 + (\Delta C_{Primed}/\Delta C_{Ctrl}) \quad (5)$$

Values of PEF > 1 and PEF < 1 denote positive and negative priming effects, respectively. This framework allowed the evaluation of temperature-dependent modulation of SOC degradation and algal-induced priming intensity.

2.5 Microbial community analysis with 16S rRNA gene high throughput sequencing and data processing

Total genomic DNA was extracted from approximately 0.5 g of wet sediment using the FastDNA Spin Kit for Soil (MP Biomedicals, Solon, OH, USA) following the manufacturer's instructions. DNA concentration and purity were assessed using a NanoDrop spectrophotometer (Thermo Fisher Scientific, USA), and structural integrity was verified by agarose gel electrophoresis. Extracted DNA samples were then frozen at -80 °C until high-throughput sequencing, which was run by Novogen Co. Ltd. (Beijing, China). The V4-V5 hypervariable region of the bacterial 16S rRNA gene was amplified using universal primers 515F (5′-GTGCCAGCMGCCGCGGTAA-3′) and 907R (5′-CCGTCAATTCCTTTGAGTTT-3′) (Xiong et al., 2012). The PCR reactions were carried out in a 20 μL reaction mixture containing 15 μL of Phusion® High-Fidelity PCR Master Mix (New England Biolabs), 2 μM of each primer, and 10 ng of template DNA. The PCR thermal cycling conditions consisted of an initial denaturation at 98 °C for 1 min; 30 cycles of 98 °C for 10 s, 50 °C for 30 s, and 72 °C for 30 s; and a final extension at 72 °C for 5 min. PCR products were pooled in equimolar ratios and purified using AMPure XP beads (Beckman Coulter, USA).

https://doi.org/10.5194/egusphere-2026-6752
Preprint. Discussion started: 6 November 2026
© Author(s) 2026. CC BY 4.0 License.

Sequencing libraries were constructed using the TruSeq® DNA PCR-Free Sample Preparation Kit (Illumina). Libraries were sequenced on an Illumina NovaSeq platform to generate 250 bp paired-end reads. Raw reads were quality-filtered and denoised using the DADA2 (Callahan et al., 2016) algorithm implemented in QIIME2 (version 2022.2). High-quality sequences were resolved into amplicon sequence variants (ASVs) at 100% sequence identity. Representative sequences were assigned taxonomy against the SILVA database (v138.1, Quast et al., 2013).

2.6 Statistical analysis

Data visualization was performed using OriginPro 2025, and the ggplot2 package in R (version 4.5.1) was used for graphics. All statistical analyses were performed in R and SPSS (version 22.0), with significance evaluated at the 95% confidence level (alpha = 0.05). Data normality was assessed visually using histograms and Q-Q plots. Statistical significance was assessed using type II analysis of variance (ANOVA). For microbial community profiling, statistical analyses of QIIME2-processed sequence data were conducted in R using the vegan package based on normalized ASV abundances. Differences in the relative abundance of dominant taxa among treatments were evaluated using two-way ANOVA. Alpha diversity indices, including Shannon diversity and Pielou's evenness, were calculated to assess community richness and evenness. Beta diversity was assessed using Bray-Curtis dissimilarities, visualized with principal coordinates analysis (PCoA), and tested for treatment differences with permutational multivariate analysis of variance (PERMANOVA/ADONIS).

Microbial co-occurrence networks were constructed separately for the control (n=12) and algae-amended (n=9) groups using samples collected across different incubation temperatures and sampling times. Spearman rank correlations ($|\rho| \geq 0.85$, $p < 0.01$) were used to identify co-occurrence associations. The networks were constructed using the igraph package in R and visualized in Gephi (v0.10.1). Keystone taxa were identified based on Betweenness Centrality and degree values. Functional potentials were predicted using PICRUSt2 (Douglas et al., 2020). Finally, relationships between environmental variables and bacterial community composition (at the phylum level) were examined using Spearman rank correlations and redundancy analysis (RDA) via the vegan package (Chen et al., 2026).

3. Results

3.1 Output of sediment microbial fuel cells (SMFCs) during the incubation

Under open-circuit conditions, the voltages of SMFCs in control and treatment groups increased progressively before reaching stabilization (Fig. 2). The maximum voltages reached 311-488 mV for the low temperature group (L, 25 ℃, peaking at 125-132 h, Fig. 2a), 452-514 mV for the medium temperature group (M, 30 ℃, stabilizing at ~108 h, Fig. 2b), and 251-441 mV for the high temperature group (H, 35 ℃, peaking at 84-108 h, Fig. 2c).

Under closed-circuit conditions, the overall current densities in the treatment groups were consistently higher than those in the control groups. The current densities in the control groups (LC, MC, HC) remained relatively stable at 6.9-11.2, 8.2-13.9, and 8.7-22.6 mA m^{-2}, respectively (Fig. 2a-c), showing an increasing trend with

https://doi.org/10.5194/egusphere-2026-6752
Preprint. Discussion started: 6 November 2026
© Author(s) 2026. CC BY 4.0 License.

elevated temperature (L < M < H, Fig. 2d). The treatment groups amended with algae (LT, MT, HT) exhibited five distinct phases: initial, rising, plateau, declining, and stabilized (Phases I-V, Fig. 2). Furthermore, the duration of dynamic current output increased with temperature, reaching 490 h (LT), 638 h (MT), and 741 h (HT) (Fig. 2d). Specifically, current density in LT peaked at 30.6 mA m^{-2} before stabilizing at 7.9-10.0 mA m^{-2}, while MT and HT reached higher peaks of 58.0 and 69.4 mA m^{-2}, respectively, followed by rebounds during the final stages.

3.2 The properties of overlying water and sediment

In the overlying water, POC, DOC, and DIC exhibited distinct temperature-dependent responses for both controls and treatments (Fig. 3, Table 1). POC concentrations in both controls and treatments peaked at 30 °C (2.22 mg C L^{-1} on day 13 in MC1; 1.47 mg C L^{-1} in MT1, Fig. 3a). In contrast, DOC showed a significant positive correlation with temperature in the treatment groups ($R^2 = 0.49$, $p = 0.01$, slope = 0.483; Fig. S2b), displaying a steeper accumulation rate than control groups (R^2=0.27, p=0.081, slope=0.335, Fig 3b, Fig. S2b). Algae addition further elevated DOC levels, peaking at 16.90 mg L^{-1} at 35 °C (HT4), and resulted in substantial increases in DIC up to 10.61 mM (MT3; Fig. 3c, Table 1). Furthermore, δ^{13}C-DIC values showed highly significant enrichment ($p < 0.001$, Fig. S2d, Table 1, Table S1) in algae treatments relative to controls, exceeding 13,000‰ within 10-17 days (Fig. 3d, Table 1).

In sediments, the TOC declined in the order of 30 °C group (19.6%–25.9% decrease from the initial TOC) > 35 °C group (6.3-8.0% decrease) > 25 °C group (1.9-2.5% decrease) (Fig. 3e, Table 1). Although algae addition did not significantly alter final TOC ($p > 0.05$) (Fig. S2e, Table S1), it caused significant δ^{13}C enrichment ($p < 0.001$, Fig. S2f, Table S1), peaking at 792‰ in the 35 °C + algae treatment (HT2, Fig. 3f, Table 1). This stimulation was also reflected in microbial activity: DHA increased notably following algae addition (e.g., reaching 328.55 ng TF g^{-1} h^{-1} in MT1) and remained consistently higher in the treatment groups than in their respective controls across most incubation time points (Fig. 3g, Table 1). Lignin-derived phenols (Λ_8) in the treatment groups showed a marginally significant positive correlation with temperature ($R^2 = 0.25$, $p = 0.096$, Fig. S2h), with algae-treated groups consistently displaying lower values than their respective controls (Fig. 3h, Fig. S2).

3.3 Mineralization rate and priming effects

At the end of incubation period, the base mineralization rate in the control groups responded non-linearly to temperature, peaking at 30 °C (101.39 μmol C L^{-1} d^{-1} in MC3) before declining at 35 °C (44.21 μmol C L^{-1} d^{-1} in HC4; Table 2, Fig. 4a). The mineralization rate of added ^{13}C-algae followed a similar trend: it increased 1.95-fold at 30 °C (19.36 μmol C L^{-1} d^{-1} in MT3) and dropped to a 1.56-fold the 25 °C baseline at 35 °C (15.43 μmol C L^{-1} d^{-1} in HT4 relative to 9.91 μmol C L^{-1} d^{-1} in LT2; Table 2).

Concurrently, the addition of algae altered SOC stability, shifting from negative to positive priming with warming (Table 2, Fig. 4). At 25 °C, a weak negative priming effect slightly suppressed SOC decomposition below control levels (M_{Primed}=-3.78 μmol C L^{-1} d^{-1} at day 31; Table 2). In contrast, at 30 °C and 35 °C, the coupling of warming and algae input triggered a substantial increase in total mineralization rates to

https://doi.org/10.5194/egusphere-2026-6752
Preprint. Discussion started: 6 November 2026
© Author(s) 2026. CC BY 4.0 License.

178.06 and 147.89 μmol C L^{-1} d^{-1} by the end of incubation (MT3 and HT4, respectively), driven predominantly by strong positive priming of the native SOC (M_{Primed} reaching 57.31 and 88.25 μmol C L^{-1} d^{-1}; Table 2)

The priming enhancement factor (PEF) correlated linearly with temperature (R^2 = 0.97; y = 0.22x - 4.7; Fig. 4b), crossing the unity threshold from 0.82 at 25 °C to 1.57 at 30 °C and 3.00 at 35 °C at the final sampling stage (Table 2, Fig. 4b). This indicates that while base mineralization peaked at 30 °C, the priming effect was linearly amplified by temperature across the entire investigated range.

3.4 Microbial diversity, community structure, and co-occurrence networks

The top ten dominant phyla across all incubations were *Chloroflexi* (27.5-37.6%), *Proteobacteria* (16.6-25.5%), *Firmicutes* (7.7-12.5%), *Desulfobacterota* (6.1-10.7%), *Actinobacteriota* (6.0-10.4%), *Acidobacteriota* (5.9-10.4%), *Bacteroidota* (2.8-6.0%), *Planctomycetota* (3.3-4.0%), *Campylobacterota* (0.8-2.9%), *Gemmatimonadota* (1.2-2%) (Fig. 5a). *Chloroflexi* showed a clear thermal enrichment increasing from ~28% at 25 °C to over 37% at elevated temperatures ($p<0.01$, Fig. 5a, Table S2). *Firmicutes* and *Actinobacteriota* showed moderate variations with temperature, though these shifts were not statistically significant ($p > 0.05$, Table S2). In contrast, *Desulfobacterota* was significantly suppressed by warming ($p < 0.01$, Table S2), showing a ~40% reduction at 35 °C compared to the 25 °C group, whereas *Proteobacteria* showed no significant temperature effect ($p > 0.05$, Table S2). Notably, *Bacteroidota* emerged as the primary responder to algal input, showing a statistically significant increase following algae addition ($p < 0.05$, Table S2). Algae addition triggered a ~1.3-fold increase in *Bacteroidota* relative abundance at 25 °C, rising to ~1.5-fold at 30 °C and 35 °C compared to their respective controls (Fig. 5a, Table S2). However, alpha diversity, measured using indices such as Shannon and Pielou, did not differ significantly between controls and treatments (Fig. 5b). Principal coordinate analysis (PCoA) based on Bray-Curtis dissimilarity revealed distinct shifts in bacterial community structure, primarily driven by temperature (Fig. 5c): the 25 °C community was clearly separated from the 30 °C and 35 °C communities, while the latter two communities exhibited considerable overlap. ADONIS statistically confirmed that temperature significantly influenced community composition (R^2=0.179, p = 0.001), whereas the addition of algae had no significant overall effect (R^2=0.052, p=0.110 > 0.05; Fig. 5c). When restricting PCoA analysis to 30 °C and 35 °C samples, temperature remained the dominant driver (R^2 = 0.098, p = 0.001; Fig. 5d), while algal treatment remained non-significant (R^2 = 0.072, p = 0.114; Fig. 5d). Across all temperature regimes, controls and treatments remained largely indistinguishable in multivariate space.

The co-occurrence network analysis revealed that algae treatment significantly altered the community interactome, increasing network complexity relative to the control (Fig. 6). Specifically, the network size expanded from 81 nodes and 123 edges in the control to 107 nodes and 154 edges in the algae-treated group (Fig. 6). A notable shift in interaction patterns accompanied this expansion: the proportion of positive links decreased from 70.7% to 57.1%, while negative links increased from 29.3% to 42.9%. In these networks, microbial keystone taxa were identified as highly connected nodes critical for maintaining community structure and function. Within the control sediment,

https://doi.org/10.5194/egusphere-2026-6752
Preprint. Discussion started: 6 November 2026
© Author(s) 2026. CC BY 4.0 License.

the keystone taxa consisted of *Thermoanaerobaculaceae* (ASV140), *Anaerolineaceae* (ASV16), *Marinifilaceae* (ASV39), and an unclassified member of the order *Rhizobiales* (ASV68). Following the algal amendment, the keystone taxa transitioned to a distinct functional set, including *Desulfosarcinaceae* (ASV67), an unidentified member of the class *Anaerolineae* (ASV91), *Thermoanaerobaculaceae* (ASV105), and *Anaerolineaceae* (ASV175).

3.5 Predicted microbial functions

Functional prediction via PICRUSt2 revealed distinct metabolic profiles across different treatments (Fig. 7a). In the control group, elevated temperature significantly promoted ($p < 0.05$) the biosynthesis of lipids (cis-vaccenate, gondoate, and CDP-diacylglycerol I) and branched-chain amino acids (BCAAs: L-valine, L-isoleucine I and IV). Concurrently, the rate of pyruvate fermentation to isobutanol decreased sharply ($p< 0.01$). Compared with the control, the algae-amended group exhibited a broader functional response at 35 °C. While maintaining the core trends observed in the control, the algae-amended group showed additional significant enrichment ($p < 0.05$) in aerobic respiration I, the non-oxidative pentose phosphate pathway, L-isoleucine biosynthesis III, and the incomplete reductive TCA cycle. The Z-score-standardized PICRUSt2-predicted abundance of the pyruvate fermentation to isobutanol pathway decreased with increasing temperature in both the control and algal-powder-amended groups ($P<0.01$ and $P<0.05$, respectively; Fig. 7). Heatmap clustering (Z-score > 2) at 35 °C further highlights these divergent metabolic potentials between the two groups (Fig. 7b).

3.6 Correlations between environmental factors and microbial structure and carbon mineralization

To determine links among environmental variables, microbial structure, mineralization rates, and PEF, correlation and multivariate analyses were performed (Fig. 8a). Mantel tests identified temperature as a dominant variable, showing a strong correlation with community assembly (Mantel's $r \geqslant 0.4$, $p < 0.01$). Temperature was positively correlated with DOC and (Ad/Al)s ($p < 0.01$). Community structure also correlated significantly with DOC, TOC, TN, $(Ad/Al)_v$, C/N, and native SOC sediment ($P < 0.05$), suggesting these variables are key determinants of mineralization efficiency and PEF magnitude. Spearman analysis indicated that mineralization potential was linked to temperature-driven shifts in organic matter quality. Algal amendment, which was the primary trigger for PEF, correlated highly with $\delta^{13}C$ and $\delta^{13}C$-DIC ($P < 0.001$), reflecting rapid mineralization of added substrates and their contribution to the DIC pool (Table S1).

RDA further showed that environmental variables significantly dictated community composition and mineralization dynamics (Fig. 8b; RDA1: 42.8%, RDA2: 14.5%). DIC, $\delta^{13}C$-DIC, TOC, and DHA were priority drivers of community divergence. In the RDA plot, 35 °C treatments clustered near DHA, TOC, and Λ_8. These high-activity samples were closely associated with the enrichment of *Actinobacteriota* and *Firmicutes*, implicating that these taxa were key contributors to the enhanced mineralization rate and priming effects under the warming conditions. Conversely,

https://doi.org/10.5194/egusphere-2026-6752
Preprint. Discussion started: 6 November 2026
© Author(s) 2026. CC BY 4.0 License.

Proteobacteria and *Acidobacteriota* dominated the lower-temperature treatments where mineralization rate and priming effects were less pronounced.

4. Discussion

4.1 SMFC performance reflects carbon mineralization and priming effect

Real-time voltage and current density measurements from SMFCs provided continuous and non-destructive bio-electrochemical indicators of microbial activity and sediment carbon processing, complementing conventional geochemical measurements obtained through discrete sampling (Mahmoodi Nasrabadi, 2026; Sun et al., 2024). Under open-circuit conditions, warming accelerated the development of electrogenic activity, as evidenced by the shorter time required to reach peak voltage (Fig. 2). This response is consistent with previous studies showing that elevated temperature enhanced extracellular electron transfer kinetics and microbial respiration (Martin et al., 2010; Wang et al., 2025). Importantly, oxygen sparging of the overlying water alleviated cathodic electron-acceptor limitations. Thus, the measured electrical outputs directly reflected the kinetics of anodic extracellular electron transfer associated with sediment microbial respiration, highlighting the potential of SMFCs as sensitive tools for tracking temperature-driven shifts in sediment redox processes and microbial electrogenic/metabolic activity.

Under closed-circuit conditions, distinct current trajectories revealed contrasting patterns of sediment carbon processing between treatments. In unamended controls, current densities remained relatively low and stable, reflecting baseline mineralization of native SOC, which increased moderately with temperature (Wang et al., 2025). In contrast, algae-amended treatments exhibited a multi-phase current response, characterized by an initial surge followed by secondary peaks (Fig. 2). The initial surge likely reflected the preferential utilization of readily available ^{13}C-labeled algal organic matter by electroactive microorganisms, enhancing extracellular electron transfer (Morrison et al., 2023; Zhu et al., 2024). Warming substantially prolonged elevated electrogenic activity following algal addition, suggesting sustained microbial activities beyond the transient metabolic responses typically induced by labile organic matter inputs in estuarine sediments (Xu et al., 2024). Moreover, the secondary current peaks observed at 30 and 35 °C could not be readily attributed solely to continued mineralization of the added algal substrate. When considered alongside the isotopic and geochemical evidence presented below, these late-stage responses are consistent with enhanced decomposition of more recalcitrant native SOC (e.g., Guenet et al., 2012, 2014), supporting a potential priming effect in which labile carbon inputs provide energy and metabolic resources that stimulate the decomposition of otherwise stable SOC (Kuzyakov et al., 2000; Liu et al., 2020; Schiedung et al., 2023; Yan et al., 2026; Zhou et al., 2021). However, it is important to note that SMFC output reflects extracellular electron transfer rather than total carbon utilization, therefore these signals indicate shifts in microbial metabolic activity and substrate use rather than direct quantification of sediment carbon loss.

4.2 Impacts of temperature and algal amendment on carbon mineralization and priming effect

https://doi.org/10.5194/egusphere-2026-6752
Preprint. Discussion started: 6 November 2026
© Author(s) 2026. CC BY 4.0 License.

The combined effects of warming and labile carbon input revealed a temperature-dependent shift from negative to positive priming, indicating differential regulation of intrinsic mineralization and priming processes. In the control sediments, native SOC mineralization peaked under moderate warming (30 °C) but declined at 35 °C (Table 2, Fig. 4a), suggesting that thermal stress may constrain microbial metabolism by reducing enzymatic efficiency or causing enzyme denaturation (Pan et al., 2025; Seidel et al., 2023). Mineralization of the added ^{13}C-labeled algal organic matter showed a similar decline at 35 °C (Table 2). In contrast, priming intensity increased progressively with temperature, suggesting that priming was more temperature sensitive than baseline SOC mineralization within the temperature range investigated.

The weak negative priming observed at lower temperatures (25 °C) is consistent with substrate preference theory, whereby microorganisms preferentially utilized labile carbon, thereby suppressing native SOC decomposition (Bartosiewicz et al., 2024; Bastida et al., 2019). As temperature increased, rapid hydrolysis of the algal amendment substantially increased DOC concentrations (Fig. 3b), indicating accelerated transformation of particulate organic matter into bioavailable substrates. Although thermal stress may impose physiological constraints on microbial communities (Thomson et al., 2025), the increased availability of DOC likely provided an energetic subsidy that sustained microbial metabolism, as reflected in elevated dehydrogenase activity (Fig. 3g, Table 1).

Although lignin decomposition is traditionally considered an aerobic process, recent evidence demonstrates that it can proceed efficiently under anoxic sediment conditions through extracellular electron transfer (EET) and non-enzymatic ROS-mediated pathways (e.g., Fenton-like reactions driven by reduced iron species and active anodes) (Li et al., 2025a; Bondurant et al., 2025). In our SMFC systems, the active anode acted as an inexhaustible terminal electron sink, establishing a bio-electrochemical interface that coupled electroactive microbial metabolism with continuous iron redox cycling Fe^{2+}/Fe^{3+}. This sustained electron transfer bypassed oxygen limitations and promoted the formation of ROS or reactive sulfur species (RSS) via anodic iron/sulfur cycling. Consequently, these reactive species subsequently drove the oxidative cleavage of refractory lignin structures under anoxic conditions. Warming alone accelerated this coupled bio-electrochemical cascade (as evidenced by high (Ad/Al)v/s ratios and temperature effects in Fig. S2h, Fig. S3, Table 1) by enhancing both abiotic reaction kinetics and microbial electron transfer rates (Li et al., 2025a; Bondurant et al., 2025). Furthermore, algal amendment altered the dynamics of organic matter degradation through positive priming, thereby enhancing the decomposition of vascular plant-derived organic matter (Li et al., 2025a). While TOC remained relatively stable due to concurrent algal inputs (Fig. 3e), enrichment in sedimentary δ^{13}C (Fig. 3f, Table 1) confirmed substantial incorporation of algal-derived carbon into microbial metabolic pathways. Collectively, these results support a warming-enhanced priming mechanism in which labile carbon inputs facilitate the co-metabolic decomposition of relatively refractory native SOC (Fontaine et al., 2007; Kuzyakov, 2010). Rather than uniformly accelerating carbon mineralization, warming appears to alter microbial substrate-use strategies, shifting carbon decomposition from the preferential utilization

https://doi.org/10.5194/egusphere-2026-6752
Preprint. Discussion started: 6 November 2026
© Author(s) 2026. CC BY 4.0 License.

of fresh organic inputs toward increased degradation of native SOC. This differential response has important implications for predicting the stability of mangrove carbon under the combined pressures of climate warming and eutrophication.

4.3 Microbial shifts underlying warming-amplified priming

Temperature was identified as the primary factor structuring microbial community composition, consistent with thermal filtering effects reported for coastal sediments (Vaughn et al., 2026; Zhang et al., 2025). Under warming, significant declines occurred in specific anaerobic taxa, notably a reduction in *Desulfobacterota* ($p < 0.01$, Table S2), which aligned with reports of temperature-sensitive anaerobic lineages in incubation studies (Kumar et al., 2023; Rabus et al., 2002). Conversely, the enrichment of *Chloroflexi* under warming ($p < 0.01$, Table S2) and its association with lignin-related variables in the RDA (Fig. 8b) supported that thermotolerant members within *Chloroflexi* and *Firmicutes may possess* specialized metabolic capabilities to degrade complex, aromatic carbon substrates under anaerobic conditions (Bell et al., 2022; Bovio-Winkler et al., 2023). Although some studies reported a decline in oligotrophic or K-selected taxa under thermal stress (Smith et al., 2022), we observed an increase in the relative abundance of *Actinobacteriota* following warming. The proliferation of specialized oligotrophic taxa capable of cleaving complex aromatic polymers likely enhanced the degradation of recalcitrant native SOC, aligning with the "carbon quality-temperature theory" (Li et al., 2017) and driving the observed increase in the priming enhancement factor (Fig. 4b). Simultaneously, copiotrophic groups (including specific lineages within *Firmicutes*) exhibited broader thermal tolerances (Smith et al., 2022). Their enrichment under elevated temperatures coincided with accelerated extracellular electron transfer (EET) to the anode. Rather than indicating an increase in aerobic metabolism within the anoxic sediment, this enhanced electron transfer efficiency alleviated local redox constraints and fuelled energy-intensive biosynthetic pathways, such as lipid and branched-chain amino acid (BCAA) synthesis, while downregulating lower-yield fermentation routes like pyruvate fermentation to isobutanol (Fig. 7) (Lovley, 2017). Furthermore, the enhanced anodic electron sink stimulated enzymatic and non-enzymatic oxidative pathways responsible for lignin cleavage, as evidenced by the elevated $Ad/Al_{v,s}$ ratios (Fig. S2h, Fig. S3, Table S1) (Zhang et al., 2010).

Algal addition further refined microbial community structure and interactome dynamics without drastically altering overall multivariate beta-diversity (PCoA ADONIS $p > 0.05$, Fig. 5c, d) or alpha-diversity indices (Fig. 5b). This stability indicated high functional redundancy within the resident microbiome, demonstrating that the observed priming effect was driven by metabolic activation rather than a whole community replacement. However, targeted shifts occurred at specific taxonomic and network levels. The significant enrichment of *Bacteroidota* following the addition of algae ($p<0.05$, Table S2) provided the primary energetic subsidy, as these opportunistic copiotrophs rapidly cleaved labile algal polymers (Macdonald et al., 2024; Teeling et al., 2012), thereby releasing bioavailable intermediates.

Crucially, the rise in competitive interactions (Fig. 6) points to an activated microbial biomass undergoing intense niche differentiation and competition for bioavailable nutrients and anodic electron-accepting sites, a pattern consistent with eco-

https://doi.org/10.5194/egusphere-2026-6752
Preprint. Discussion started: 6 November 2026
© Author(s) 2026. CC BY 4.0 License.

evolutionary responses observed during substrate-induced priming (Fontaine et al., 2003; Kuzyakov, 2010). Concurrently, a distinct turnover in keystone taxa occurred: while the control network was anchored by fermentative lineages (e.g., *Thermoanaerobaculaceae* ASV140, *Marinifilaceae* ASV39), the algal-amended network shifted toward *Desulfosarcinaceae* (ASV67) and *Anaerolineaceae* lineages (ASV91, ASV175). Members of *Anaerolineaceae* (*Chloroflexi*) are well recognized as hydrolytic scaffolds capable of co-metabolizing complex native aromatic structures alongside labile substrates (Yamada et al., 2006; Xia et al., 2016), whereas *Desulfosarcinaceae* facilitated interspecies electron transfer (DIET). By coupling primary organic matter hydrolysis with efficient anodic electron disposal (Rotaru et al., 2014), this syntrophic keystone module sustained high metabolic turnover, directly driving the co-metabolic breakdown of recalcitrant native SOC (priming effect).

The accumulation of DOC under warming, together with the rapid production of ^{13}C-DIC during the early incubation stage (Fig. 3d, Table 2), indicated rapid hydrolysis and mineralization of algal-derived carbon. However, elevated DOC concentrations persisted during later stages, suggesting incomplete substrate utilization. Previous studies have shown that nutrient availability, particularly phosphorus and sulfur, can constrain microbial processing of carbon inputs and regulate priming responses (Dijkstra et al., 2013; Morrison et al., 2023). Although nutrient concentrations were not directly measured in this study, the concurrent accumulation of DOC and reduced late-stage DIC production was consistent with metabolic or nutrient limitation of complete carbon oxidation (Chen et al., 2014).

Functional predictions further suggested differential microbial metabolic responses to warming. Warming alone enriched lipid biosynthesis pathways associated with cellular acclimation (Siliakus et al., 2017), whereas warming combined with algal input enriched pathways involved in respiration and central carbon metabolism (Fig. 7), indicating increased carbon processing. Incorporation of ^{13}C into bulk organic matter indicated rapid assimilation and recycling of algal-derived carbon, potentially contributing to microbial carbon pump processes (Jiao et al., 2010; Qiao et al., 2025). Together, these compositional and functional responses provide a mechanistic context for the warming-induced enhancement of positive priming observed in this study.

4.4 Implications of carbon storage sustainability in Shenzhen Bay mangroves under global changes

Mangroves and vegetated coastal habitats are considered “a natural climate solution” for sequestration of atmospheric CO_2 into stable SOC (Macreadie et al., 2021), with a global burial rate of 163 g OC m^{-2} yr^{-1} (Breithaupt et al., 2012). Mangrove SOC is believed to have a long turnover time, ranging from 4 to 36 years for the active pools and from 891 to 3,115 years for the slow-cycling pools (Zhang et al., 2013; Belshe et al., 2019). However, our findings demonstrated that acute inputs of labile algal biomass under warming conditions can transiently destabilize this recalcitrant carbon reservoir via positive priming. Based on the maximum SOC degradation rate observed in the algal-amended 30ºC treatment at 36 days (158.7 μ mol C L^{-1} d^{-1} for initial TOC of 2.24%, Table 2), the localized turnover time of active SOC pools could theoretically be shortened to approximately 5-14 years during peak disturbance events (dry sediment

https://doi.org/10.5194/egusphere-2026-6752
Preprint. Discussion started: 6 November 2026
© Author(s) 2026. CC BY 4.0 License.

density of 0.61±0.28 g cm^{-3}, Nie et al., 2026). While this value represents an upper-bound potential rate under non-limiting lab conditions rather than a steady-state annual turnover time, it underscores the vulnerability of supposedly stable blue carbon deposits to episodic biogeochemical perturbations.

Along the coastline of Shenzhen Bay, mangrove areal coverage is now expanding as a consequence of protection and restoration projects (Feng et al., 2020; Wang et al., 2021). However, this increase in organic carbon production may not lead to long-term carbon storage if the priming mechanisms are intensified by climate and anthropogenic disturbances. For example, increasing runoff from urbanized watersheds has intensified nitrogen and phosphorus loading into Shenzhen Bay (Wang et al., 2024), triggering coastal eutrophication and red tides (Xu et al., 2019). This enhanced deposition of nutrient-rich algal material into mangrove organic sediments may intensify positive priming of organic carbon degradation, as observed in the current study, thereby degrading the coastal carbon sink. Nevertheless, many uncertainties need to be addressed to further investigate this impact. For instance, Shenzhen Bay has experienced oxygen depletion due to nutrient loading and harmful algal blooms (Qian et al., 2018; Zhou et al., 2020). Shifts in water-column oxygen availability may restructure microbial consortia and affect degradation rates. Furthermore, sea-level rise and nutrient loading are now changing the spatial distribution, reproduction, and productivity of Shenzhen Bay mangroves (Huang et al., 2023; He et al., 2025), altering the amount and quality of litter production that serves as the native substrate for priming reactions.

5. Conclusion

This study demonstrates that warming differentially regulates baseline carbon mineralization and priming in mangrove sediments. While baseline native SOC mineralization peaked under moderate warming (30 °C) but declined under thermal stress (35 °C), the addition of labile algal carbon sustained microbial activity and progressively amplified positive priming across the entire temperature range. These findings revealed that fresh, bioavailable carbon inputs provided energetic subsidies that stimulated the co-metabolic decomposition of previously recalcitrant SOC under anoxic conditions. Mechanistically, our findings highlight that sediment carbon stability under global change is governed by substrate availability, microbial substrate-use strategies, and redox constraints rather than temperature alone.

The integration of sediment microbial fuel cells (SMFCs) with ^{13}C isotope tracing proved to be a powerful, non-destructive bio-electrochemical approach for continuously tracking microbial metabolic activities in carbon cycles. By serving as an inexhaustible terminal electron sink, the SMFC anode enabled electroactive microorganisms to sustain oxidative pathways—such as lignin cleavage—even within anoxic sediment matrices.

Because priming intensity exhibited greater temperature sensitivity than baseline SOC respiration, predictive biogeochemical models that represent sediment carbon loss solely as a direct function of temperature-dependent processes substantially underestimate blue carbon vulnerability in eutrophic coastal ecosystems. Incorporating microbial priming processes and substrate-dependent carbon turnover into predictive

https://doi.org/10.5194/egusphere-2026-6752
Preprint. Discussion started: 6 November 2026
© Author(s) 2026. CC BY 4.0 License.

frameworks should improve projections of blue carbon persistence under future climate change.

CRediT authorship contribution statement

Conceptualization: XL, JK
Funding acquisition: XL
Investigation: WN, JK, XL
Methodology: WN, JK, XL
Formal analysis: WN, GZ, XL
Visualization: WN, JK, XL
Supervision: XL, JK
Project administration: XL
Writing-original draft: all
Writing-review & editing: all

Declaration of competing interest

The authors declare that they have no known competing financial interests or personal relationships that could have appeared to influence the work reported in this paper.

Acknowledgements

This work was supported by the National Natural Science Foundation of China (42576030, 42276045), Guangdong Overseas Distinguished Scholar Project (MS202500134), High Level Special Fund of Southern University of Science and Technology (G03050K001), Shenzhen Marine Development Research Promotion Center (SZDL2023000925, SZDL2024001761), Shenzhen Natural Resources and Real Estate Evaluation and Development Research Center, and Endowment from Stroud Water Research Center.

Data availability

Data related to this article can be found in the paper and Supplemental Materials.

All sequence data have been deposited in the NCBI Sequence Read Archive under accession number PRJNA1542023.

https://doi.org/10.5194/egusphere-2026-6752
Preprint. Discussion started: 6 November 2026
© Author(s) 2026. CC BY 4.0 License.

References

Aller, R.C., Cochran, J.K., 2019. The critical role of bioturbation for particle dynamics, priming potential, and organic carbon remineralization in marine sediments: Local and basin scales. Frontiers in Earth Science 7, 157.

Ali, S., Dey, G., Nuong, N.H.K., Rahman, A., Wang, L.C., Sukul, U., Das, K., Sharma, R.K., Wang, S.L., Chen, C.Y., 2025. Carbon sequestration in mangrove ecosystems: Sources, transportation pathways, influencing factors, and its role in the carbon budget. Earth-Science Reviews 269, 105184.

Alongi, D.M., 2014. Carbon cycling and storage in mangrove forests. Annual Review of Marine Science 6, 195-219.

Bartosiewicz, M., Przytulska, A., Birkholz, A., Zopfi, J., Lehmann, M.F., 2024. Controls and significance of priming effects in lake sediments. Global Change Biology 30, e17076.

Bastida, F., García, C., Fierer, N., Eldridge, D.J., Bowker, M.A., Abades, S., Alfaro, F.D., Asefaw Berhe, A., Cutler, N.A., Gallardo, A., García-Velázquez, L., Hart, S.C., Hayes, P.E., Hernández, T., Hseu, Z.-Y., Jehmlich, N., Kirchmair, M., Lambers, H., Neuhauser, S., Peña-Ramírez, V.M., Pérez, C.A., Reed, S.C., Santos, F., Siebe, C., Sullivan, B.W., Trivedi, P., Vera, A., Williams, M.A., Moreno, J.L., Delgado-Baquerizo, M., 2019. Global ecological predictors of the soil priming effect. Nature Communications 10, 3481.

Bell, E., Rattray, J.E., Sloan, K., Sherry, A., Pilloni, G., Hubert, C.R.J., 2022. Hyperthermophilic endospores germinate and metabolize organic carbon in sediments heated to 80°C. Environmental Microbiology 24, 5534-5545.

Belshe, E.F., Sanjuan, J., Leiva-Dueñas, C., Piñeiro-Juncal, N., Serrano, O., Lavery, P., Mateo, M.A., 2019. Modeling organic carbon accumulation rates and residence times in coastal vegetated ecosystems. Journal of Geophysical Research: Biogeosciences 124, 3652-3671.

Bengtsson, M.M., Attermeyer, K., Catalán, N., 2018. Interactive effects on organic matter processing from soils to the ocean: Are priming effects relevant in aquatic ecosystems? Hydrobiologia 822, 1-17.

Bengtsson, M.M., Wagner, K., Burns, N.R., Herberg, E.R., Wanek, W., Kaplan, L.A., Battin, T.J., 2014. No evidence of aquatic priming effects in hyporheic zone microcosms. Scientific Reports 4, 5187.

Bianchi T.S., 2011. The role of terrestrially derived organic carbon in the coastal ocean: A changing paradigm and the priming effect, Proceedings of the National Academy of Sciences 108(49), 19473–19481.

Bianchi, T.S., Thornton, D.C.O., Yvon-Lewis, S.A., King, G.M., Eglinton, T.I., Shields, M.R., Ward, N.D., Curtis, J., 2015. Positive priming of terrestrially derived dissolved organic matter in a freshwater microcosm system. Geophysical Research Letters 42, 5460-5467.

Bianchi, T.S., Cui, X.Q., Blair, N., Burdige, D.J., Eglinton, T.I., Galy, V., 2018. Centers of organic carbon burial and oxidation at the land-ocean interface, Organic Geochemistry 115, 138-155.

Bondurant, L.C., Baker, M.L., Hage, S., Talling, P.J., Hatcher, P.G., 2025. Variations in lignin content deposited in the Congo Fan and its potential for oxidative degradation. Marine Chemistry 273, 104569.

Bonin P., Portas A., Hardy J., Guasco S., Bianchi T.S., Ward N.D., Rontani J.F. 2023. Biological mechanisms underlying priming of vascular plant material in the presence of diatoms. Aquatic Microbial Ecology 89, 99-117.

Bovio-Winkler, P., Guerrero, L.D., Erijman, L., Oyarzúa, P., Suárez-Ojeda, M.E., Cabezas, A., Etchebehere, C., 2023. Genome-centric metagenomic insights into the role of Chloroflexi in anammox, activated sludge and methanogenic reactors. BMC Microbiology 23, 45.

https://doi.org/10.5194/egusphere-2026-6752
Preprint. Discussion started: 6 November 2026
© Author(s) 2026. CC BY 4.0 License.



751 Breithaupt, J.L., Smoak, J.M., Smith III, T.J., Sanders, C.J., Hoare, A., 2012. Organic carbon burial
752 rates in mangrove sediments: Strengthening the global budget. Global Biogeochemical Cycles 26,
753 GB3011.
754 Callahan, B.J., McMurdie, P.J., Rosen, M.J., Han, A.W., Johnson, A.J.A., Holmes, S.P., 2016. DADA2:
755 High-resolution sample inference from Illumina amplicon data. Nature Methods 13, 581-583.
756 Catalán, N., Kellerman, A.M., Peter, H., Carmona, F., Tranvik, L.J., 2015. Absence of a priming effect
757 on dissolved organic carbon degradation in lake water. Limnology and Oceanography 60, 159-168.
758 Chen, R., Senbayram, M., Blagodatsky, S., Myachina, O., Dittert, K., Lin, X., Blagodatskaya, E.,
759 Kuzyakov, Y., 2014. Soil C and N availability determine the priming effect: microbial response to glucose
760 and ammonium addition. Soil Biology and Biochemistry 78, 223–231.
761 Chen, S., Wu, H., Xu, W., Wang, F., Yan, R., Li, S., Chen, N., 2026. Biogenic carbon input from *Spartina*
762 *alterniflora* eradication governs nitrate removal pathways and N2O emission in estuarine mangrove
763 wetlands. Geoderma 468, 117780.
764 Danger, M., Cornut, J., Chauvet, E., Chavez, P., Elger, A., Lecerf, A., 2013. Benthic algae stimulate
765 leaf litter decomposition in detritus-based headwater streams: A case of aquatic priming effect?,
766 Ecology 94(7), 1604–1613.
767 Dijkstra, F. A., Carrillo, Y., Pendall, E., Morgan, J. A., 2013. Rhizosphere priming: a review of studies
768 on C and N dynamics under elevated CO_2. Soil Biology and Biochemistry 57, 911–920.
769 Donato, D.C., Kauffman, J.B., Murdiyarso, D., Kurnianto, S., Stidham, M., Kanninen, M., 2011.
770 Mangroves among the most carbon-rich forests in the tropics. Nature Geoscience 4, 293-297.
771 Dong, H., Lin, J., Lu, J., Li, L., Yu, Z., Kumar, A., Zhang, Q., Liu, D., Chen, B., 2024. Priming effects of
772 surface soil organic carbon decreased with warming: A global meta-analysis. Plant and Soil 500, 233-
773 242.
774 Feng, Z., Tan, G., Xia, J., Shu, C., Chen, P., Wu, M., Wu, X., 2020. Dynamics of mangrove forests in
775 Shenzhen Bay in response to natural and anthropogenic factors from 1988 to 2017. Journal of Hydrology
776 591, 125271.
777 Fontaine, S., Barot, S., Barré, P., Bdioui, N., Mary, B., Rumpel, C., 2007. Stability of organic
778 carbon in deep soil layers controlled by fresh carbon supply. Nature 450, 277–280.
779 Fontaine, S., Mariotti, A., Abbadie, L., 2003. The priming effect of organic matter: a question
780 of microbial competition? Soil Biology and Biochemistry 35(6), 837–843.
781 Gontikaki, E., Thornton, B., Huvenne, V.A.I., Witte, U., 2013. Negative priming effect on organic
782 matter mineralisation in NE Atlantic slope sediment, PLoS One 8(6), e67722.
783 Gontikaki, E., Thornton, B., Cornulier, T., Witte, U., 2015. Occurrence of priming in the
784 degradation of lignocellulose in marine sediments. PLoS ONE 10, e0143917.
785 Guenet, B., Danger, M., Abbadie, L., Lacroix, G., 2010. Priming effect: Bridging the gap between
786 terrestrial and aquatic ecology. Ecology 91, 2850–2861.
787 Guenet, B., Danger, M., Harrault, L., Allard, B., Jauset-Alcala, M., Bardoux, G., Benest, D., Abbadie,
788 L., Lacroix, G., 2014. Fast mineralization of land-born C in inland waters: first experimental evidences of
789 aquatic priming effect. Hydrobiologia 721(1), 35-44.
790 Guenet, B., Juarez, S., Bardoux, G., Abbadie, L., Chenu, C., 2012. Evidence that stable C is as
791 vulnerable to priming effect as is more labile C in soil. Soil Biology and Biochemistry 52, 43-48.
792 Guo, C., Loh, P.S., Hu, J., Chen, Z., Pradit, S., Oeurng, C., Sok, T., Mohamed, C.A.R., Lee, C.W., Bong,
793 C.W., Lu, X., Anshari, G.Z., Kandasamy, S., Wang, J., 2024. Factors influencing mangrove carbon storage
794 and its response to environmental stress. Frontiers in Marine Science 11, 1410183.

https://doi.org/10.5194/egusphere-2026-6752
Preprint. Discussion started: 6 November 2026
© Author(s) 2026. CC BY 4.0 License.

Halewood, E., Opalk, K., Custals, L., Carey, M., Hansell, D.A., Carlson, C.A., 2022. Determination of dissolved organic carbon and total dissolved nitrogen in seawater using High Temperature Combustion Analysis. Frontiers in Marine Science 9, 1061646.

He, Q., Wu, X., Huang, Y., Ma, E., Yang, J., Wang, J., 2025. Spatiotemporal evolution of shorelines in Shenzhen Bay (1986–2020): Contrasting impacts of rapid urbanization in Shenzhen and natural processes in Hong Kong. Frontiers in Marine Science 12, 1695029.

Hedges, J.I., Ertel, J.R., 1982. Characterization of lignin by gas capillary chromatography of cupric oxide oxidation products. Analytical Chemistry 54, 174-178.

Huang, Z., Li, Z., Wang, M., Zhu, D., Yang, Q., Yu, S., 2023. Coastal nutrient enrichments facilitated reproductive output in exotic mangrove species over two decades. Frontiers in Forests and Global Change 6, 1183432.

IPCC, 2022. The Ocean and Cryosphere in a Changing Climate: Special Report of the Intergovernmental Panel on Climate Change. Cambridge University Press, Cambridge.

Jiao, N., Herndl, G.J., Hansell, D.A., Benner, R., Kattner, G., Wilhelm, S.W., Kirchman, D.L., Weinbauer, M.G., Luo, T., Chen, F., Azam, F., 2010. Microbial production of recalcitrant dissolved organic matter: Long-term carbon storage in the global ocean. Nature Reviews Microbiology 8, 593-599.

Kan, J., Hsu, L., Cheung, A.C.M., Pirbazari, M., Nealson, K.H., 2011. Current production by bacterial communities in microbial fuel cells enriched from wastewater sludge with different electron donors. Environmental Science & Technology 45, 1139-1146.

Kumar, S., Najar, I.N., Sharma, P., Tamang, S., Mondal, K., Das, S., Sherpa, M.T., Thakur, N., 2023. Temperature – A critical abiotic paradigm that governs bacterial heterogeneity in natural ecological system. Environmental Research 234, 116547.

Kuzyakov, Y., 2010. Priming effects: Interactions between living and dead organic matter. Soil Biology and Biochemistry 42(9), 1363–1371.

Kuzyakov, Y., Friedel, J.K., Stahr, K., 2000. Review of mechanisms and quantification of priming effects. Soil Biology and Biochemistry 32, 1485-1498.

Li, J.Q., Pei, J.M., Cui, J., Chen, X.P., Li, B., Nie, M., Fang, C.M., 2017. Carbon quality mediates the temperature sensitivity of soil organic carbon decomposition in managed ecosystems, Agriculture, Ecosystems & Environment 250, 44-50.

Li, J., Sun, W., Cao, Y., Wu, J., Duan, L., Zhang, M., Luo, X., Deng, Q., Peng, Z., Mou, X., Li, W., Wang, P., 2025. Increased temperature enhances microbial-mediated lignin decomposition in river sediment. Microbiome 13, 89.

Li, P., Xiong, Y., Lu, B., Hu, B., Wu, S., Duan, L., Zhang, H., 2025. Carbon credit assessment for mangrove conservation: A detailed study of Futian Mangrove reserve in Shenzhen. Marine Environmental Research 210, 107255.

Li, X., Feng, J., Zhang, Q., Zhu, B., 2023. Warming inhibits the priming effect of soil organic carbon mineralization: A meta-analysis. Science of The Total Environment 904, 166170.

Liu, X.J., Finley, B.K., Mau, R.L., Schwartz, E., Dijkstra, P., Bowker, M.A., Hungate, B.A., 2020. The soil priming effect: Consistent across ecosystems, elusive mechanisms, Soil Biology and Biochemistry 140, 107617.

Lovley, D.R., 2017. Happy together: microbial communities that hook up to swap electrons. The ISME Journal 11(2), 327–336.

Löhnis, F., 1926. Nitrogen availability of green manures, Soil Science 22(4), 253–290.

Macdonald, J.F.H., Pérez-García, P., Schneider, Y.K.H., Blümke, P., Indenbirken, D., Andersen, J.H.,

https://doi.org/10.5194/egusphere-2026-6752
Preprint. Discussion started: 6 November 2026
© Author(s) 2026. CC BY 4.0 License.

Krohn, I., Streit, W.R., 2024. Community dynamics and metagenomic analyses reveal Bacteroidota's role in widespread enzymatic *Fucus vesiculosus* cell wall degradation. Scientific Reports 14, 10237.

Macreadie, P.I., Anton, A., Raven, J.A., Beaumont, N., Connolly, R.M., Friess, D.A. et al., 2019. The future of Blue Carbon science, Nature Communications 10(1), 3998.

Macreadie, P.I., Costa, M.D.P., Atwood, T.B., Friess, D. A., Kelleway, J. J., Kennedy, H., Lovelock, C.E., Serrano, O., Duarte, C.M., 2021. Blue carbon as a natural climate solution. Nature Reviews Earth & Environment **2**, 826–839.

Mahmoodi Nasrabadi, A., 2026. A detailed survey of microbial fuel cells: Classifications, computational modeling, recent innovations, and emerging applications. Renewable and Sustainable Energy Reviews 226, 116241.

Malone, T.C., Newton, A., 2020. The globalization of cultural eutrophication in the coastal ocean: Causes and consequences. Frontiers in Marine Science 7, 670.

Martin, E., Savadogo, O., Guiot, S.R., Tartakovsky, B., 2010. The influence of operational conditions on the performance of a microbial fuel cell seeded with mesophilic anaerobic sludge. Biochemical Engineering Journal 51, 132-139.

Morrison, E.S., Liu, Y., Rivas-Ubach, A., Amaral, J.H.F., Shields, M., Osborne, T.Z., Chu, R., Ward, N., Bianchi, T.S., 2023. Mangrove peat and algae leachates elicit rapid and contrasting molecular and microbial responses in coastal waters. Communications Earth & Environment 4, 376.

Nie T.Y., Zhou K., Zhang F., Zhai X.H., Li W.P., Wang H.W., Sun C.P., Kang Z.J., Hu X.P., Ning W.F., Qi Y.F., Chen J.Z., Li X.X., 2026. Spatial heterogeneity and controls of sedimentary organic carbon distribution in different types of coastal wetland, CATENA 273, 110409.

Paerl, H.W., Hall, N.S., Peierls, B.L., Rossignol, K.L., 2014. Evolving paradigms and challenges in estuarine and coastal eutrophication dynamics in a culturally and climatically stressed world. Estuaries and Coasts 37, 243-258.

Pan, J., Zheng, X., Liao, D., Jiang, Z., Li, X., Li, C., Li, Y., Zhao, J., Ma, X., Geng, Q., Zhang, C., Wu, Q., Dong, Z., 2025. Temperature fluctuation affects soil organic carbon accumulation through soil enzyme activity and nutrient limitation. Environmental Technology & Innovation 40, 104458.

Qian, W., Gan, J., Liu, J., He, B., Lu, Z., Guo, X., Wang, D., Guo, L., Huang, T., Dai, M., 2018. Current status of emerging hypoxia in a eutrophic estuary: The lower reach of the Pearl River Estuary, China. Estuarine, Coastal and Shelf Science 205, 58-67.

Qiao, L., Wang, J., Wei, S., Ren, Y., Lichtfouse, E., Han, J., 2025. The soil microbial carbon pump for carbon sequestration. Environmental Chemistry Letters 23, 1145-1151.

Quast, C., Pruesse, E., Yilmaz, P., Gerken, J., Schweer, T., Yarza, P., Peplies, J. and Glöckner, F.O., 2012. The SILVA ribosomal RNA gene database project: improved data processing and web-based tools. Nucleic Acids Research 41(D1), D590–D596.

Rabus, R., Brüchert, V., Amann, J., Könneke, M., 2002. Physiological response to temperature changes of the marine, sulfate-reducing bacterium *Desulfobacterium autotrophicum*. FEMS Microbiology Ecology 42, 409-417.

Regnier, P., Resplandy, L., Najjar, R.G., Ciais, P., 2022. The land-to-ocean loops of the global carbon cycle. Nature 603, 401-410.

Reimers, C.E., Tender, L.M., Fertig, S., Wang, W., 2001. Harvesting energy from the marine sediment-water interface. Environmental Science & Technology 35, 192-195.

Rotaru, A.E., Shrestha, P.M., Liu, F., Markovaite, B., Chen, S., Nevin, K.P., Lovley, D.R., 2014. Direct interspecies electron transfer in methanogenic aggregates/syntrophic consortia. Energy &

https://doi.org/10.5194/egusphere-2026-6752
Preprint. Discussion started: 6 November 2026
© Author(s) 2026. CC BY 4.0 License.

Environmental Science 7(1), 408–415.

Sang, W., Yang, H., Feng, W., Chen, H., Tang, J., Chen, S., 2026. Unlocking the impact of temperature and salinity on greenhouse gas emissions from estuarine salt marsh soils. Earth's Future 14, e2025EF006912.

Schiedung, M., Don, A., Beare, M.H., Abiven S., 2023. Soil carbon losses due to priming moderated by adaptation and legacy effects. Nature Geoscience 16, 909–914.

Seidel, L., Broman, E., Nilsson, E., Ståhle, M., Ketzer, M., Pérez-Martínez, C., Turner, S., Hylander, S., Pinhassi, J., Forsman, A., Dopson, M., 2023. Climate change-related warming reduces thermal sensitivity and modifies metabolic activity of coastal benthic bacterial communities. The ISME Journal 17, 855-869.

Siliakus, M.F., van der Oost, J., Kengen, S.W.M., 2017. Adaptations of archaeal and bacterial membranes to variations in temperature, pH and pressure. Extremophiles 21, 651-670.

Smith, T.P., Mombrikotb, S., Ransome, E., Kontopoulos, D.G., Pawar, S., Bell, T., 2022. Latent functional diversity may accelerate microbial community responses to temperature fluctuations. eLife 11, e80867.

Song, N., Jiang, H.-L., 2018. Effects of initial sediment properties on start-up times for sediment microbial fuel cells. International Journal of Hydrogen Energy 43, 10082-10093.

Sun, F., Chen, J., Tang, M., Yang, Y., 2024. Recent research progress, challenges and future directions of sediment microbial fuel cell: A comprehensive review. International Journal of Hydrogen Energy 50, 870-886.

Teeling, H., Fuchs, B.M., Becher, D., Klockow, C., Gardebrecht, A., Bennke, C.M., Kassabgy, M., Huang, S., Mann, A.J., Waldmann, J., Weber, M., Klindworth, A., Otto, A., Lange, J., Bernhardt, J., Reinsch, C., Hecker, M., Peplies, J., Bockelmann, F.D., Callies, U., Gerdts, G., Wichels, A., Wiltshire, K.H., Glöckner, F.O., Schweder, T., Amann, R., 2012. Substrate-controlled succession of marine bacterioplankton populations induced by a phytoplankton bloom. Science 336, 608-611.

Thomson, T., Pilditch, C.A., Fusi, M., Prinz, N., Lundquist, C.J., Ellis, J.I., 2025. Vulnerability of Labile Organic Matter to Eutrophication and Warming in Temperate Mangrove Ecosystems. Global Change Biology 31, e70087.

van Nugteren, Moodley, P.L., Brummer, G., Heip, C.H., Herman, P.M., and Middelburg, J.J., 2009. Seafloor ecosystem functioning: The importance of organic matter priming, Marine Biology 156(11), 2277–2287.

Vaughn, S.N., Pavlovsky, J.C., Heiman, J.A., Jackson, C.R., 2026. Contrasting spatial and temporal structuring of seawater and sediment bacterial communities in coastal environments. Scientific Reports 16, 14586.

Wang, C.T., Vasumathi, K., Tumboimbela, J.R.W., Das, B., Tritanti, J.S., Wu, C., 2025. Temperature-driven changes in biofilm formation and electrochemical performance of deep-sea inoculum in microbial fuel cells. Bioelectrochemistry 166, 109012.

Wang, H., Peng, Y., Wang, C., Wen, Q., Xu, J., Hu, Z., Jia, X., Zhao, X., Lian, W., Temmerman, S., Wolf, J., Bouma, T., 2021. Mangrove loss and gain in a densely populated urban estuary: Lessons from the Guangdong-Hong Kong-Macao Greater Bay Area. Frontiers in Marine Science 8, 693450.

Wang, Y., Feng, W., Li, X., Luo, H., Xu, W., Xu, X., Wang, H., Chen, Y., 2024. Analysis of nitrogen and phosphorus pollution in Shenzhen Bay over the past 40 years. Water 16, 3002.

Xia, Y., Wang, Y., Wang, Y., Chin, F.Y., Zhang, T., 2016. Cellular evidence supports *Anaerolineae* as key players in organic matter degradation. Environmental Microbiology 18(9), 3000–3014.

Xiong, J., Liu, Y., Lin, X., Zhang, H., Zeng, J., Hou, J., Yang, Y., Yao, T., Knight, R., Chu, H., 2012.

https://doi.org/10.5194/egusphere-2026-6752
Preprint. Discussion started: 6 November 2026
© Author(s) 2026. CC BY 4.0 License.



Geographic distance and pH drive bacterial distribution in alkaline lake sediments across Tibetan Plateau. Environmental Microbiology 14, 2457-2466.

Xu, H., Zhang, Y., Zhu, X., Zheng, M., 2019. Effects of rainfall-runoff pollution on eutrophication in coastal zone: A case study in Shenzhen Bay, southern China. Hydrology Research 50, 1062-1075.

Xu, M., Wang, X., Xi, R., Long, Y., Kou, J., Liu, X., 2018. Characteristics of nutrients and eutrophication assessment of Shenzhen offshore waters. IOP Conference Series: Earth and Environmental Science 153, 062038.

Xu, M., Wang, Y., Feng, Z., Wu, H., 2024. Rapid variations of phytoplankton blooms and their dynamics off the Changjiang River Estuary. Frontiers in Marine Science 11, 1345940.

Yamada, C., Sekiguchi, Y., Hanada, S., Imachi, H., Ohashi, A., Harada, H., Kamagata, Y. 2006. Anaerolinea thermophila gen. nov., sp. nov. and *Pelolinea- Anaerolineaceae* lineages as key degraders of complex organic matter. International Journal of Systematic and Evolutionary Microbiology 56(4), 731–740.

Yan, Q., Cheng, T., Song, J., Zhou, J., Hung, C.-C., Cai, Z., 2021. Internal nutrient loading is a potential source of eutrophication in Shenzhen Bay, China. Ecological Indicators 127, 107736.

Yan, S., Yin, L., He, Y., Wang, X., Wang, P., 2026. Persistent soil organic carbon is more susceptible to the priming effect than labile soil organic carbon. Soil Ecology Letters 8(6), 260484.

Yang, J., Han, M., Zhao, Z., Jiang, H., 2022. Positive priming effects induced by allochthonous and autochthonous organic matter input in the lake sediments with different salinity. Geophysical Research Letters 49, e2021GL096133.

Zhang, J.P., Yi, W.X., Shen, C.D., Ding, P., Ding, X.F., Fu, D.P., Liu, K.X., 2013. Quantification of sedimentary organic carbon storage and turnover of tidal mangrove stands in southern China based on carbon isotopic measurements. Radiocarbon 55, 1665-1674.

Zhang, T., Gannon, S.M., Nevin, K.P., Franks, A.E., Lovley, D.R., 2010. Stimulating the anaerobic degradation of aromatic hydrocarbons and complex organic matter by providing solid-state electron acceptors. Environmental Science & Technology 44(10),3853–3858.

Zhang, Y., Gao, X., Shao, Z., Sun, Y., Zhang, Z., Li, H., Ye, J., 2025. Latitude-dependent diversity and assembly processes of coastal microbial communities across multiple trophic levels in the China Seas. Frontiers in Marine Science 12, 1714451.

Zhou, J., Wen, Y., Shi, L.L., Marshall, M.R., Kuzyakov, Y., Blagodatskaya, E., Zang, H.D., 2021. Strong priming of soil organic matter induced by frequent input of labile carbon, Soil Biology and Biochemistry 152, 108069.

Zhou, Y., Wang, L., Zhou, Y., Mao, X.Z., 2020. Eutrophication control strategies for highly anthropogenic influenced coastal waters. Science of The Total Environment 705, 135760.

Zhu, D., Cheng, X., Sample, D.J., Qiao, Q., Liu, Z., 2023. Effect of water temperature on internal nitrogen release from sediments in the Pearl River Delta region, China. Hydrology Research 54, 1055-1071.

Zhu, Q.Z., Yin, X., Taubner, H., Wendt, J., Friedrich, M.W., Elvert, M., Hinrichs, K.-U., Middelburg, J.J., 2024. Secondary production and priming reshape the organic matter composition in marine sediments. Science Advances 10, eadm8096.

https://doi.org/10.5194/egusphere-2026-6752
Preprint. Discussion started: 6 November 2026
© Author(s) 2026. CC BY 4.0 License.

Table 1. Biogeochemical parameters of overlying water and sediments during SMFC incubation across different temperatures.

Treatment	Group ID	Incubation days	Overlying water				Sediments								
			POC (mg C L^{-1})	DOC (mg·L^{-1})	DIC (mM)	δ^{13}C-DIC (‰)	TOC (%)	δ^{13}C (‰)	TN (%)	δ^{15}N (‰)	C/N	DHA (ng TF·g^{-1}·h^{-1})	Λ_8 (mg/100 mg OC)	$(Ad/Al)_V$	$(Ad/Al)_S$
25 °C	LC0	10	1.20	6.63	3.20	-2.07	1.57	-25.01	0.19	8.32	9.50	173.11	1.33	0.1438	0.0784
	LC1	17	0.83	6.64	3.37	-2.78	1.59	-25.41	0.19	8.74	9.78	222.15	2.37	0.1692	0.0858
	LC2	31	0.73	6.22	3.85	31.92	1.54	-25.14	0.19	8.68	9.44	179.17	1.67	0.1577	0.0867
25 °C + Algae	LT1	17	0.70	9.69	4.24	15393	1.57	514	0.18	8.15	10.00	249.74	1.31	0.1616	0.0825
	LT2	31	1.13	8.14	4.04	33825	1.53	679	0.19	7.53	9.40	190.86	1.5	0.1659	0.0889
30 °C	MC0	10	1.08	8.66	4.20	-0.99	2.24	-26.93	0.24	8.18	10.94	313.99	2.07	0.2001	0.0893
	MC1	13	2.22	13.07	7.04	-5.21	2.28	-26.70	0.24	8.60	11.15	215.43	2.32	0.1797	0.0926
	MC2	17	1.07	8.73	5.48	-1.90	1.72	-25.47	0.22	8.21	9.15	168.23	1.68	0.1704	0.0941
	MC3	36	0.81	15.15	7.85	3.08	1.66	-25.96	0.21	8.45	9.41	154.43	1.83	0.1733	0.0989
30 °C + Algae	MT1	13	1.47	9.09	2.89	18400	2.2	323	0.23	8.29	11.39	328.55	2.1	0.201	0.1003
	MT2	17	1.42	11.05	6.81	29261	1.65	479	0.19	8.26	9.95	172.32	1.97	0.205	0.1178
	MT3	36	1.13	13.87	10.61	29197	1.8	368	0.25	6.85	8.52	177.60	1.66	0.1915	0.1028
35 °C	HC0	7	1.30	10.62	4.31	2.89	1.75	-26.04	0.19	8.83	10.48	255.81	2.37	0.185	0.093
	HC1	10	0.75	9.53	5.34	-2.89	1.74	-25.40	0.19	8.84	10.71	276.25	1.85	0.1923	0.1008
	HC2	12	0.79	10.24	4.47	3.21	1.68	-26.13	0.19	8.84	10.57	178.44	1.79	0.1756	0.0919
	HC3	18	0.88	9.85	6.29	-3.59	1.63	-25.91	0.18	8.74	10.70	185.18	2.89	0.1806	0.0877
	HC4	38	0.61	11.56	5.99	-1.77	1.61	-24.84	0.18	8.93	10.39	158.39	1.67	0.1872	0.1064
35 °C + Algae	HT1	10	0.70	11.39	3.55	13286	1.69	539	0.20	8.17	9.94	289.33	1.63	0.1864	0.0998
	HT2	12	1.05	12.61	3.13	17418	1.7	792	0.20	8.14	10.04	273.90	1.71	0.1916	0.1014
	HT3	18	1.35	13.49	6.52	25932	1.75	302	0.19	8.35	10.35	183.04	1.72	0.1844	0.1001
	HT4	38	1.13	16.90	9.93	26250	1.64	321	0.19	8.43	10.75	180.81	1.69	0.1804	0.1021

Note: POC: particulate organic carbon; DOC: dissolved organic carbon; DIC: dissolved inorganic carbon; δ^{13}C-DIC: stable carbon isotope of dissolved inorganic carbon; TOC: total organic carbon; δ^{13}C: stable carbon isotope; TN: total nitrogen; C/N: atomic ratio of carbon to nitrogen; δ^{15}N: stable nitrogen isotope; DHA: Dehydrogenase activity; Λ_8: lignin-derived phenols; $(Ad/Al)_S$: acid-to-aldehyde ratio of S-series lignin monomers; $(Ad/Al)_V$: acid-to-aldehyde ratio of V-series lignin monomers.

https://doi.org/10.5194/egusphere-2026-6752
Preprint. Discussion started: 6 November 2026
© Author(s) 2026. CC BY 4.0 License.

Table 2. DIC content from different sources in culture systems and mineralization rate of organic carbon at various time points under different incubation temperatures.

Treatment	Group ID	Incubation days	C_f (mM)	C_i (mM)	ΔC_{Ctrl} (mM)	ΔC_{Primed} (mM) [a]	ΔC_A (mM) [a]	$\delta^{13}C_f$ (‰)	$\delta^{13}C_i$ (‰)	$\delta^{13}C_{Ctrl}$ (‰)	$\delta^{13}C_{sed,\ amended}$ (‰)	$\delta^{13}C_A$ (‰)	$M_{Control}$ (μ mol C $L^{-1}d^{-1}$) [a]	M_{Primed} (μ mol C $L^{-1}d^{-1}$) [a]	M_A (μ mol C $L^{-1}d^{-1}$) [a]	PEF [a]
25	LC0	10	3.2	3.2	0	n/a	n/a	-2.07	-2.07	-25.01	n/a	n/a	0	n/a	n/a	n/a
	LC1	17	3.37	3.2	0.17	n/a	n/a	-2.78	-2.07	-25.41	n/a	n/a	10	n/a	n/a	1.00
	LC2	31	3.85	3.2	0.65	n/a	n/a	31.92	-2.07	-25.14	n/a	n/a	20.97	n/a	n/a	1.00
25 °C + Algae	LT1	17	4.24	3.2	0.17	0.72	0.15	15393	-2.07	-25.41	514	444739	10	42.54	8.64	5.25
	LT2	31	4.04	3.2	0.65	-0.12	0.31	33825	-2.07	-25.14	679	444739	20.97	-3.78	9.91	0.82
30	MC0	10	4.2	4.2	0	n/a	n/a	-0.99	-0.99	-26.93	n/a	n/a	0	n/a	n/a	n/a
	MC1	13	7.04	4.2	2.84	n/a	n/a	-5.21	-0.99	-26.70	n/a	n/a	218.46	n/a	n/a	1.00
	MC2	17	5.48	4.2	1.28	n/a	n/a	-1.90	-0.99	-25.47	n/a	n/a	75.29	n/a	n/a	1.00
	MC3	36	7.85	4.2	3.65	n/a	n/a	3.08	-0.99	-25.96	n/a	n/a	101.39	n/a	n/a	1.00
30 °C + Algae	MT1	13	2.89	4.2	2.84	-4.27	0.12	18400	-0.99	-26.70	323	444739	218.46	-328.42	9.19	-0.50
	MT2	17	6.81	4.2	1.28	0.88	0.45	29261	-0.99	-25.47	479	444739	75.29	51.87	26.36	1.69
	MT3	36	10.61	4.2	3.65	2.06	0.70	29197	-0.99	-25.96	368	444739	101.39	57.31	19.36	1.57
35	HC0	7	4.31	4.31	0	n/a	n/a	2.89	2.89	-26.04	n/a	n/a	0	n/a	n/a	n/a
	HC1	10	5.34	4.31	1.03	n/a	n/a	-2.89	2.89	-25.40	n/a	n/a	103	n/a	n/a	1.00
	HC2	12	4.47	4.31	0.16	n/a	n/a	3.21	2.89	-26.13	n/a	n/a	13.33	n/a	n/a	1.00
	HC3	18	6.29	4.31	1.98	n/a	n/a	-3.59	2.89	-25.91	n/a	n/a	110	n/a	n/a	1.00
	HC4	38	5.99	4.31	1.68	n/a	n/a	-1.77	2.89	-24.84	n/a	n/a	44.21	n/a	n/a	1.00
35 °C + Algae	HT1	10	3.55	4.31	1.03	-1.90	0.11	13286	2.89	-25.40	539	444739	103	-189.60	10.60	-0.84
	HT2	12	3.13	4.31	0.16	-1.46	0.12	17418	2.89	-26.13	792	444739	13.33	-121.87	10.21	-8.14
	HT3	18	6.52	4.31	1.98	-0.15	0.38	25932	2.89	-25.91	303	444739	110	-8.35	21.12	0.92
	HT4	38	9.93	4.31	1.68	3.35	0.59	26250	2.89	-24.84	321	444739	44.21	88.25	15.43	3.00

Note: a: Calculated values. n/a: Not applicable for control groups without algae addition. C_i: Initial DIC concentrations; C_f: Final DIC concentrations; ΔC_{Ctrl}: DIC production from control sediments under a given temperature; ΔC_A: DIC derived from algal organic matter mineralization; ΔC_{Primed}: Additional DIC production induced by priming effects; $M_{Control}$: Mineralization rate of sediment organic carbon in control group; M_{Primed}: Mineralization rate of primed sediment organic carbon; M_A: Mineralization rate of algae; PEF: Priming enhancement factor.

https://doi.org/10.5194/egusphere-2026-6752
Preprint. Discussion started: 6 November 2026
© Author(s) 2026. CC BY 4.0 License.

Figures

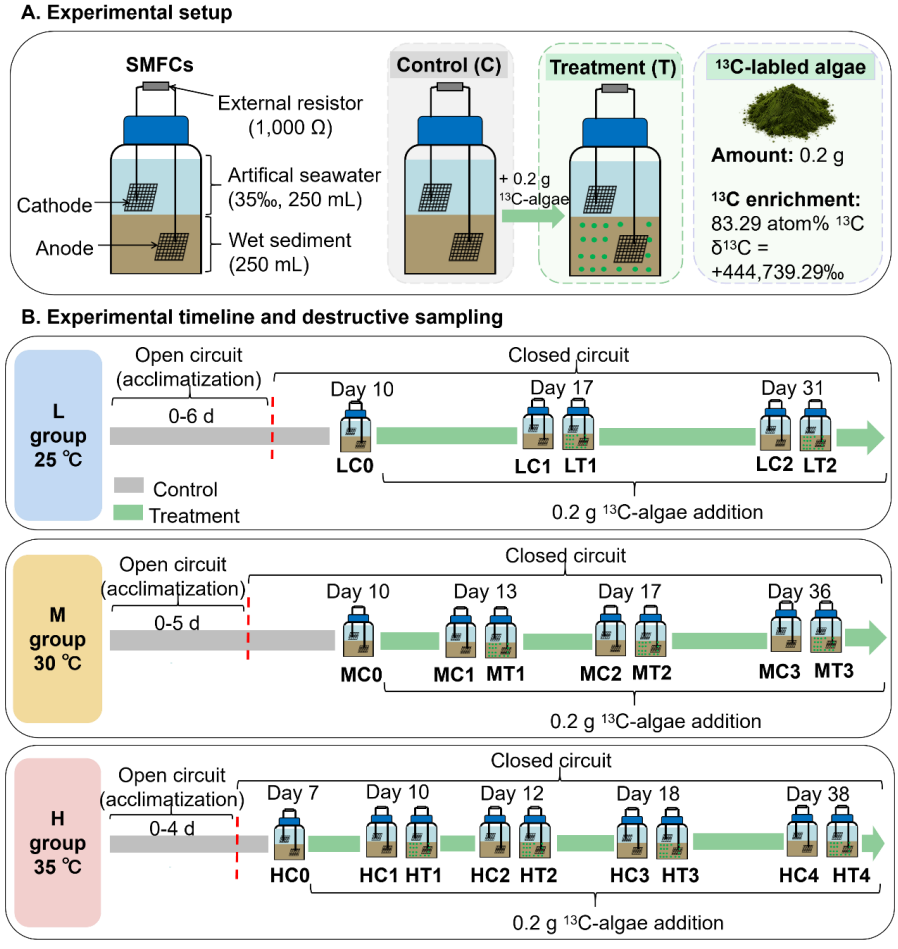


Fig. 1. Schematic illustration of the sediment microbial fuel cells (SMFCs) experimental setup and sampling design under three temperature conditions (25, 30, and 35 °C). Following open-circuit acclimation, baseline samples (C0) were collected after circuit closure but before the addition of ^{13}C-labeled algae, with one SMFC sampled at each temperature (n = 1). Control (C) and algae-amended (T) SMFCs were subsequently destructively sampled at temperature-specific time points, with one SMFC sampled per treatment at each time point (n = 1).

https://doi.org/10.5194/egusphere-2026-6752
Preprint. Discussion started: 6 November 2026
© Author(s) 2026. CC BY 4.0 License.

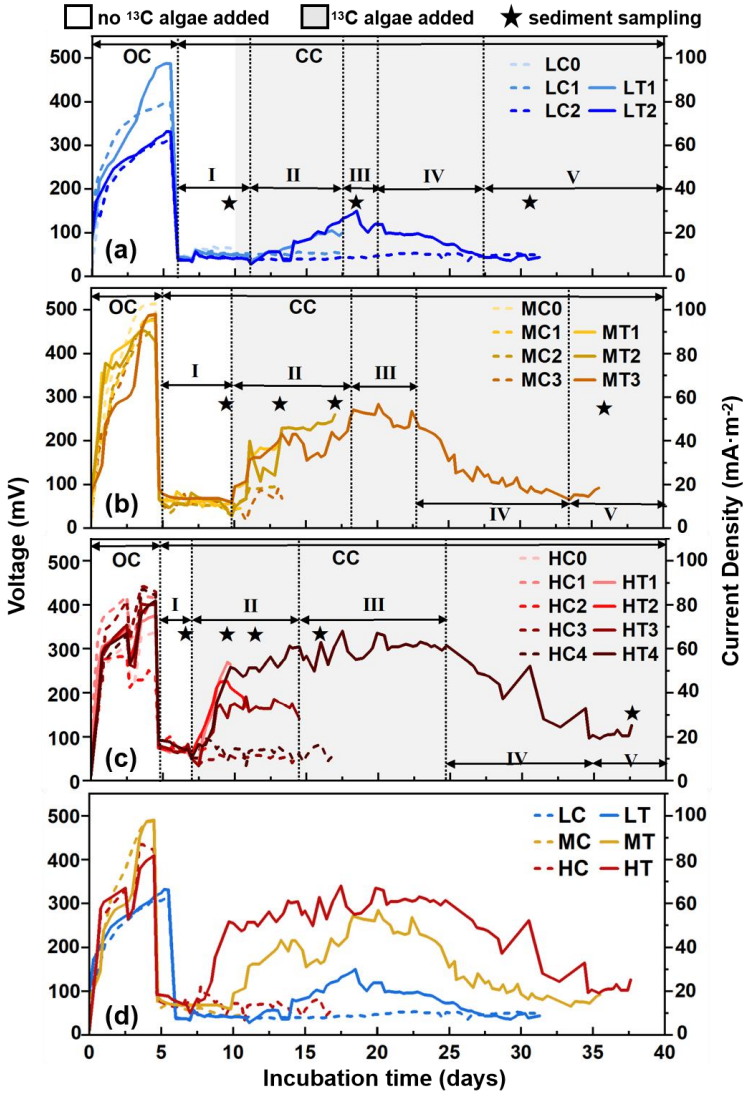


Fig. 2. Voltage and current density in sediment microbial fuel cells (SMFCs) over incubation time under different temperatures: low (L, 25 °C; a), medium (M, 30 °C; b), and high (H, 35 °C; c). Corresponding control (C) and treatment (T) experiments were conducted with destructive sampling at selected time points. All SMFCs were initially operated under open-circuit conditions, and algal amendments were then added to the treatments (T) after the onset of the closed-circuit stage. (d) Continuous incubation experiment without destructive sampling. I: Initial phase; II: Growth phase; III: Plateau phase; IV: Decline phase; V: Final phase. The sampling points LC0-2, LT1-2, MC0-3, MT1-3, HC0-4, and HT1-4 are labeled over incubation time as shown in Figure 1. OC: Open Circuit; CC: Closed Circuit. Voltage is referenced to the left axis; the right-axis current-density scale applies only to the closed-circuit stage.

https://doi.org/10.5194/egusphere-2026-6752
Preprint. Discussion started: 6 November 2026
© Author(s) 2026. CC BY 4.0 License.

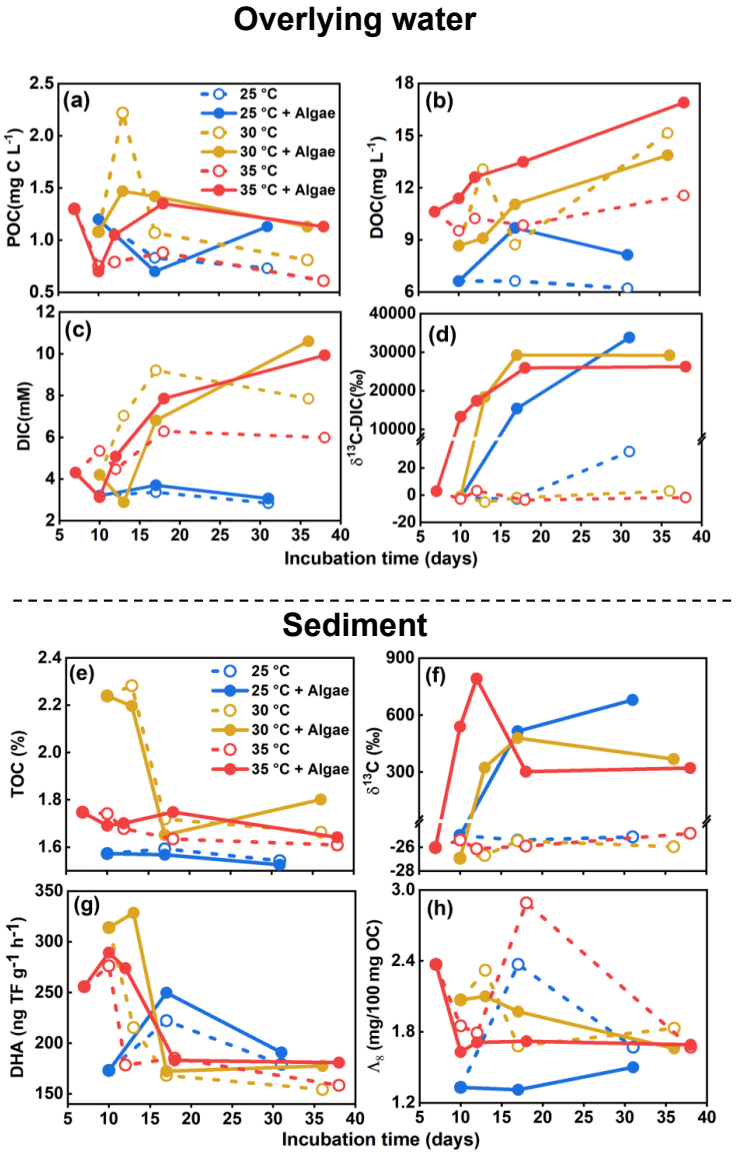


Fig. 3. Variation trends of (a) particulate organic carbon (POC), (b) dissolved organic carbon (DOC), (c) dissolved inorganic carbon (DIC), and (d) stable carbon isotope of dissolved inorganic carbon (δ^{13}C-DIC) in the overlying water and (e) total organic carbon, (f) stable carbon isotope (δ^{13}C), (g) Dehydrogenase activity (DHA), and (h) lignin-derived phenols (Λ_8) of sediment samples during incubation time.

https://doi.org/10.5194/egusphere-2026-6752
Preprint. Discussion started: 6 November 2026
© Author(s) 2026. CC BY 4.0 License.

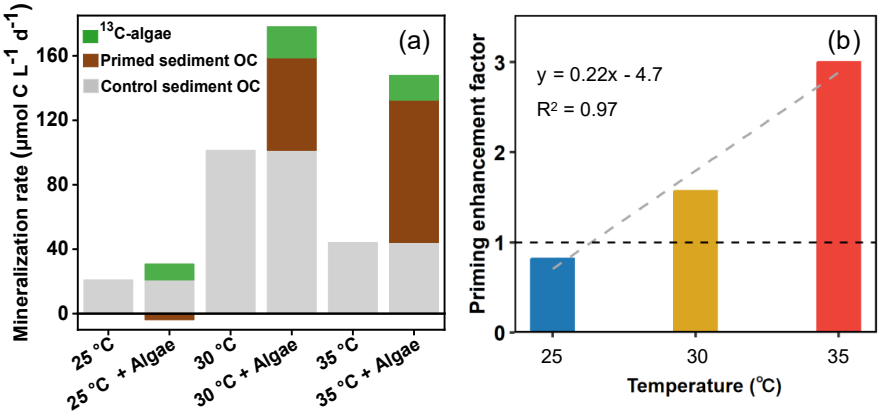
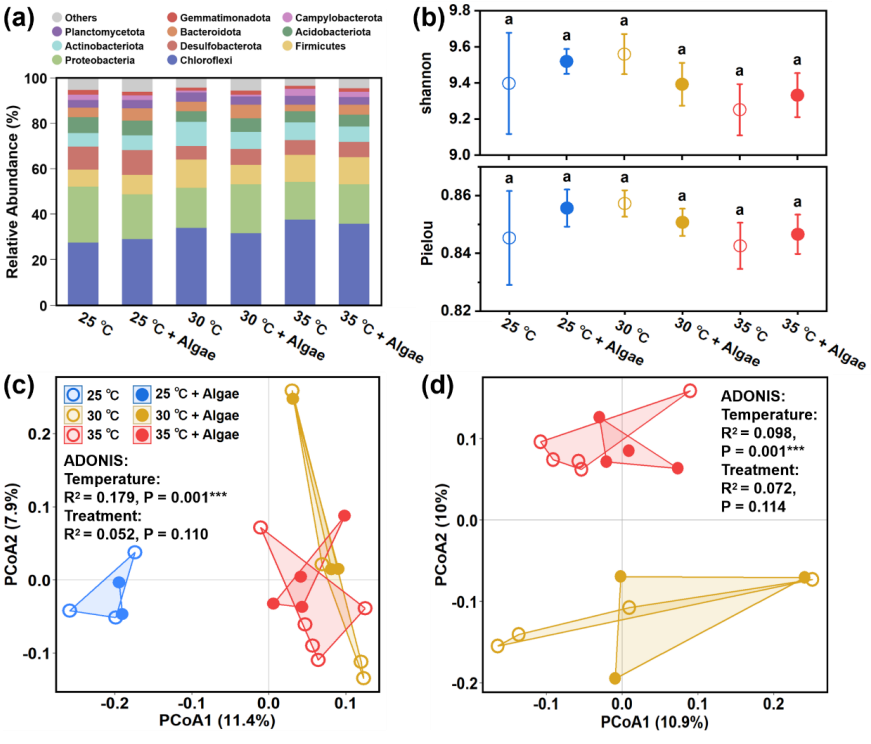


Fig. 4. (a) Mineralization rate of organic carbon in the control sediment, primed sediment organic carbon, and priming substrates (e.g., ^{13}C-algae) based on the end-member mixing model for each treatment. **(b)** Impact of temperature on the priming enhancement factor (mineralization rate of sediment organic carbon in primed treatments divided by that in the control at respective temperature) following algae addition. The grey dashed line represents the linear regression between temperature and the priming enhancement factor. The horizontal black dashed line at y=1 indicates the threshold between negative priming (< 1) and positive priming (> 1).



https://doi.org/10.5194/egusphere-2026-6752
Preprint. Discussion started: 6 November 2026
© Author(s) 2026. CC BY 4.0 License.

Fig. 5. (a) Relative abundance of the top 10 microbial phyla in sediments across different temperatures and treatments. **(b)** Diversity characteristics of microbial communities for sediment samples across different temperatures and treatments. **(c)** Principal coordinate analysis (PCoA) of the microbial community composition for each temperature and algal amendment based on Bray–Curtis dissimilarity. The effects of temperature and algal amendments were assessed using an ADONIS analysis. P-values show the level of significance, and R^2 statistic values display the degree of discrimination. **(d)** PCoA analysis of microbial community composition restricted to 30℃ and 35℃ samples.

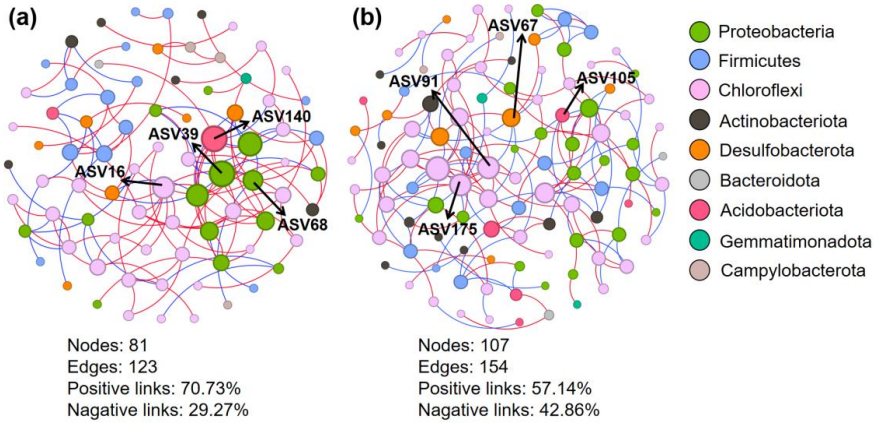


Fig. 6. Co-occurrence networks of species-level microbial community; **(a)** Control, **(b)** Algal amendment. The ASVs in the figures represent the keystone taxa. A connection stands for a strong (Spearman's correlation coefficient $|\rho| \geq 0.85$) and significant ($p < 0.01$) correlation between two ASVs. The different colors of the nodes indicate different phyla. The size of the node represents the number of connections (i.e., degree). The blue lines indicate negative interactions, while red lines indicate positive interactions.

https://doi.org/10.5194/egusphere-2026-6752
Preprint. Discussion started: 6 November 2026
© Author(s) 2026. CC BY 4.0 License.

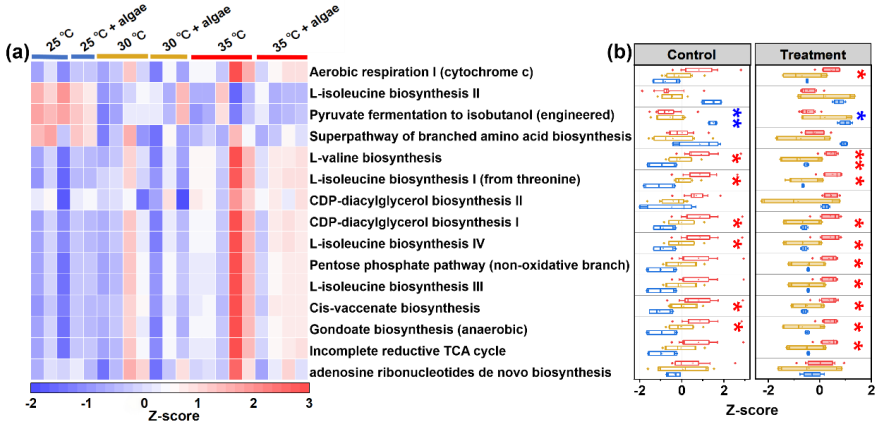


Fig. 7. (a) Comparative analysis of group-specific metabolic pathways. Predicted metabolic pathway abundances inferred by PICRUSt2 are displayed as a Z-score heatmap. The Z-score for each pathway within a group signifies its deviation from the overall mean abundance: Z-score = 0 (abundance equal to mean), Z-score > 0 (red, enriched abundance, with increasing values indicating stronger enrichment), Z-score < 0 (blue, depleted abundance, with decreasing values indicating stronger suppression). **(b)** The box charts depict variations in metabolic function across different conditions. Asterisks indicate significant differences among temperature groups based on the Kruskal-Wallis test (*$p < 0.05$). Red and blue asterisks indicate significantly increased and decreased abundances of predicted pathways, respectively, in response to elevated temperature.

https://doi.org/10.5194/egusphere-2026-6752
Preprint. Discussion started: 6 November 2026
© Author(s) 2026. CC BY 4.0 License.

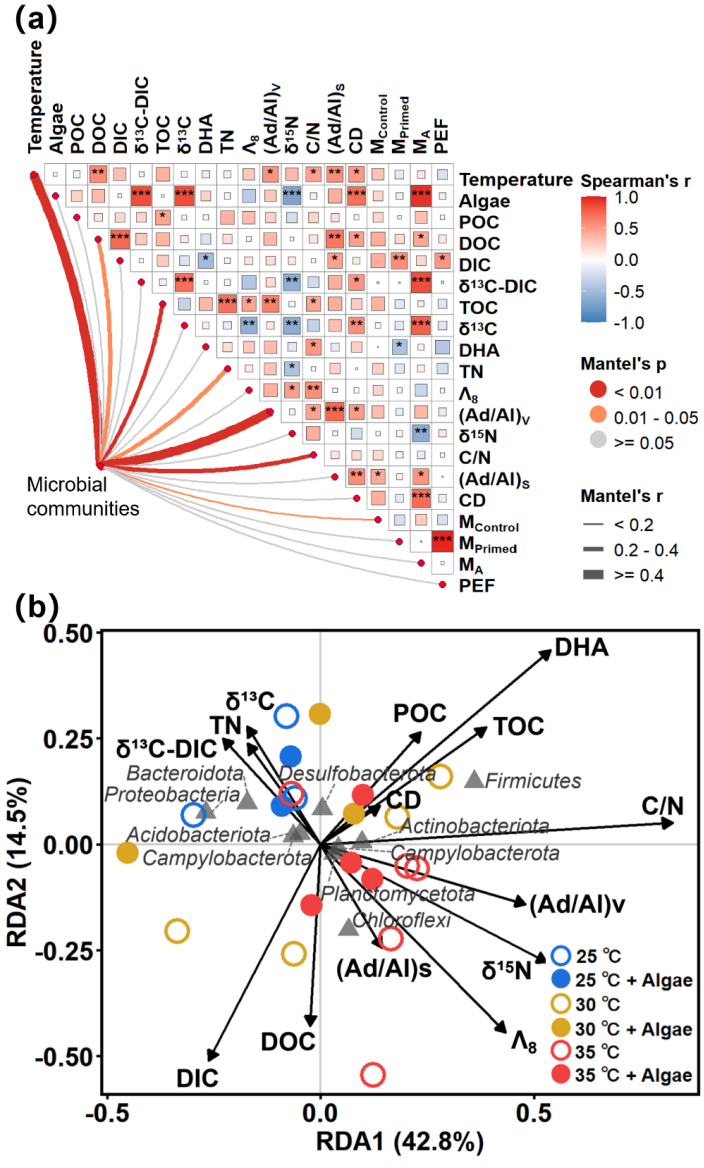


Fig. 8. (a) Mantel tests and Spearman correlations showing relationships between environmental variables (overlying water physicochemical properties and sediment parameters), microbial communities, and mineralization rates. The Mantel's r statistic is represented by line width, and the color of the circle indicates the statistical significance; square colors indicate Spearman's r. Asterisk means the relation is significant (*p < 0.05, **p < 0.01, and ***p < 0.001). CD: current density; PEF: priming enhancement factor. **(b)** Redundancy analysis between biogeochemical parameters and microbial composition (phylum-level).